Origin of Coda Waves: source, attenuation and scattering effects

Article *in* Journal of Geophysical Research: Solid Earth · August 1975

DOI: 10.1029/JB080i023p03322

2 authors, including:

B. Chouet
United States Geological Survey
183 PUBLICATIONS **13,800** CITATIONS

SEE PROFILE

Origin of Coda Waves: Source, Attenuation, and Scattering Effects

KEIITI AKI AND BERNARD CHOUET

Department of Earth and Planetary Sciences, Massachusetts Institute of Technology, Cambridge, Massachusetts 02139

Coda waves from small local earthquakes are interpreted as backscattering waves from numerous heterogeneities distributed uniformly in the earth's crust. Two extreme models of the wave medium that account for the observations on the coda are proposed. In the single backscattering model the scattering is considered to be a weak process, and the loss of seismic energy by scattering is neglected. In the diffusion model the seismic energy transfer is considered as a diffusion process. Both models lead to similar formulas that allow an accurate separation of the effect of earthquake source from the effects of scattering and attenuation on the coda spectra. A unique difference was found in the scaling law of earthquake source spectra between central California and western Japan, which may be attributed to the difference in inhomogeneity length of the earth's crust. The Q of coda waves in the two regions is strongly frequency dependent with values increasing from 50–200 at 1 Hz to about 1000–2000 at 20 Hz. This observation is interpreted as a combined effect of variation of Q with depth and frequency-dependent composition of coda waves described below. The turbidity coefficient of the lithosphere required at 1 Hz to explain the observed coda as body wave scattering is orders of magnitude greater than previously known values such as those obtained by Aki (1973) and Capon (1974) under the Montana Lasa from the amplitude and phase fluctuations of teleseismic P waves. From the high attenuation and turbidity obtained at this frequency we conclude that at around 1 Hz the coda is made of backscattering surface waves from heterogeneities in the shallow, low-Q lithosphere. The high Q observed for the coda at frequencies higher than 10 Hz, on the other hand, eliminates the possibility that these waves are backscattering surface waves. We conclude that at these high frequencies the coda must be made of backscattering body waves from heterogeneities in the deep lithosphere. The low turbidities found for deep earthquake sources under western Japan are consistent with this model of coda wave generation.

INTRODUCTION

The subject of this paper is high-frequency seismic waves in the range up to 25 Hz coming from small local earthquakes. These high-frequency waves are fascinating because of their sensitivity to the details of seismic source and the earth's structure.

In order to exploit the potential sensitivity of these waves to the details of seismic source and wave path we must be able to interpret the seismograms in terms of parameters of their physical models. A straightforward deterministic interpretation is difficult because of the extreme sensitivity of these waves to details. Numerical methods such as the finite difference and finite element methods may be used in special cases in which the model parameters for the earth medium are known and the computer cost is not a factor. This is, however, not the case in the usual study of local earthquakes.

The above difficulties may be avoided by resorting to a statistical treatment of the heterogeneity of the earth medium. In other words, a small number of statistical parameters may be sufficient to characterize the medium for interpreting a certain aspect of the seismograms. There have been several attempts in recent years along this direction in earthquake seismology [*Aki*, 1969, 1973; *Takano* 1971; *Haddon*, 1972; *Cleary and Haddon*, 1972; *King et al.*, 1973; *Capon*, 1974], and explosion seismology [*Wesley*, 1965; *Nikolayev*, 1968; *Nikolayev and Tregub*, 1970; *Levin and Robinson*, 1969; *Dunkin*, 1969; *Greenfield*, 1971], as well as lunar seismology [*Nakamura et al.*, 1970; *Dainty et al.*, 1974*a*].

The longer the waves travel, the greater the variety of heterogeneities they encounter. The later portions of a seismogram therefore may be considered as a result of some kind of averaging over many samples of heterogeneities, thus suggesting a statistical treatment in which a small number of parameters characterize the average properties of the heterogeneous medium.

A few years ago *Aki* [1969] suggested that the seismic coda waves of local earthquakes are backscattering waves from numerous randomly distributed heterogeneities in the earth and may be treated by a statistical method. The observational data accumulated since then by us and others in this country, Norway, and Japan seem to support that assumption. A recent study by *Scheimer and Landers* [1974] has also confirmed the validity of Aki's model.

In this paper we shall first present evidence for supporting our assumption that the coda waves are backscattering waves from randomly distributed heterogeneities. Then we shall describe the method of interpreting the observed coda spectra on the basis of the single-scattering theory as well as the diffusion theory. The method will be applied to the data obtained in Japan and California by using a spectral analyzing seismograph of *Tsujiura* [1966, 1967, 1969].

An accurate separation of source, attenuation, and scattering effects on the coda spectra will lead us to the discovery of a significantly different scaling law of earthquake source spectra for different seismic areas. A coherent picture of the nature of coda waves emerges from the quantitative analysis of the scattering and attenuation properties. We shall conclude that at around 1 Hz they are backscattering surface waves from heterogeneities in the shallow, low-Q part of the earth's crust. On the other hand, for frequencies higher than 10 Hz they are primarily backscattering body waves from heterogeneities in the deep, high-Q lithosphere.

ORIGIN OF THE CODA OF LOCAL EARTHQUAKES

Coda waves studied in this paper are the tail of a seismogram (after the arrival of major wave types such as P, S, and surface waves) recorded at a short distance from an earthquake. Let us first enumerate several important facts about the coda waves.

1. The spectral contents of the early part of a local earth-

quake seismogram depend strongly on the travel distance and the nature of the wave path to a station. The difference in spectrum among stations, however, diminishes in the later part of the seismogram and disappears in the coda [e.g., *Aki*, 1956, 1969].

2. For a given local earthquake at epicentral distance shorter than about 100 km the total duration of a seismogram (the length of time from the beginning of *P* waves to the end of coda) is nearly independent of the epicentral distance or azimuth and can be used effectively as a measure of earthquake magnitude [*Bisztricsany*, 1958; *Soloviev*, 1965; *Tsumura*, 1967; *Lee et al.*, 1972].

3. The power spectra of coda waves from different local earthquakes decay as a function of time (measured from the earthquake origin time) in the same manner independent of the distance and the nature of the path between epicenter and station [*Aki*, 1969; this paper].

4. The above time dependence (3) is also independent of the earthquake magnitude, at least for small earthquakes with $M < 6$ [*Aki*, 1969; this paper].

5. The coda excitation depends, however, on the local geology of the station site. It can be 5–8 times larger on the sediment than on granite [*Aki*, 1969]. Interestingly, the amplitude of ambient ground noise tends to be proportional to the site factor of coda excitation, making the total duration recognized on the records for various sites nearly independent of local geology.

6. The study of coda by a small-aperture array of seismographs shows that they are not regular plane waves coming from the epicenter [*Aki et al.*, 1958; *Aki and Tsujiura*, 1959; *Scheimer and Landers*, 1974].

Three major origins of coda that immediately come to our minds are (1) slow surface waves due to low-velocity sediment and/or water bodies such as ponds and lakes, (2) waves generated by the aftershocks at the earthquake source, and (3) backscattering by heterogeneities distributed in the large region outside the zone of the direct wave path from the source to the station.

First, the 'slow wave' model cannot explain the items 1, 2, 3, and 4 in the list of observed facts described above. The clearest evidence against this model can be seen in Figure 1 of *Aki* [1969], in which the equality of coda spectra is demonstrated between stations located within 1–2 km from the epicenters and those at 15–18 km away. The short-period records of a local earthquake at Norsar (Figure 1 of this paper) further demonstrate the independence of coda power decay on the nature of wave path between the earthquake source and various subarray locations, as well as on the epicentral distance which ranges from a few kilometers to more than 100 km in this case.

The 'aftershock' model may be refuted on the following two accounts. The item 2 on the list of observed facts, that the total duration serves as the measure of earthquake magnitude, can be explained if the aftershocks last longer for greater earth-

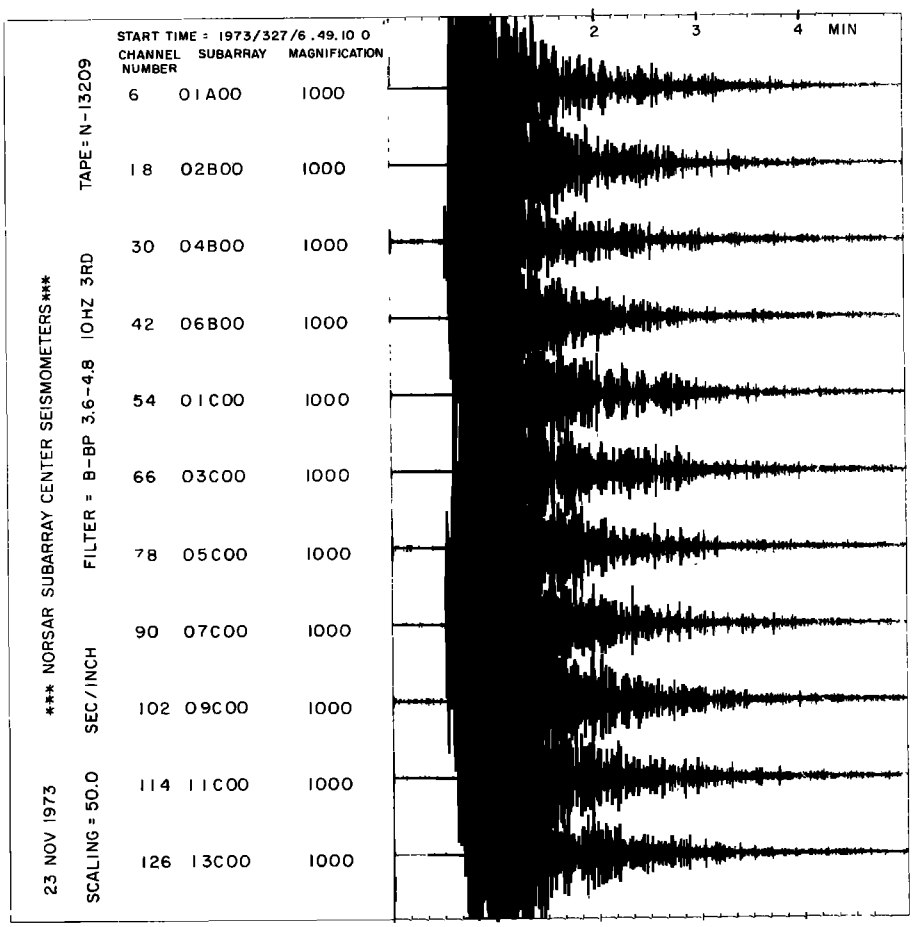

Fig. 1. Short-period (band pass from 3.6 to 4.8 Hz) records of a local earthquake at Norsar near subarray 7C. The epicentral distance is a few kilometers to the closest subarray and more than 100 km to the farthest. The decay of coda power shows no dependence on the details of the different wave paths between the earthquake source and each subarray.

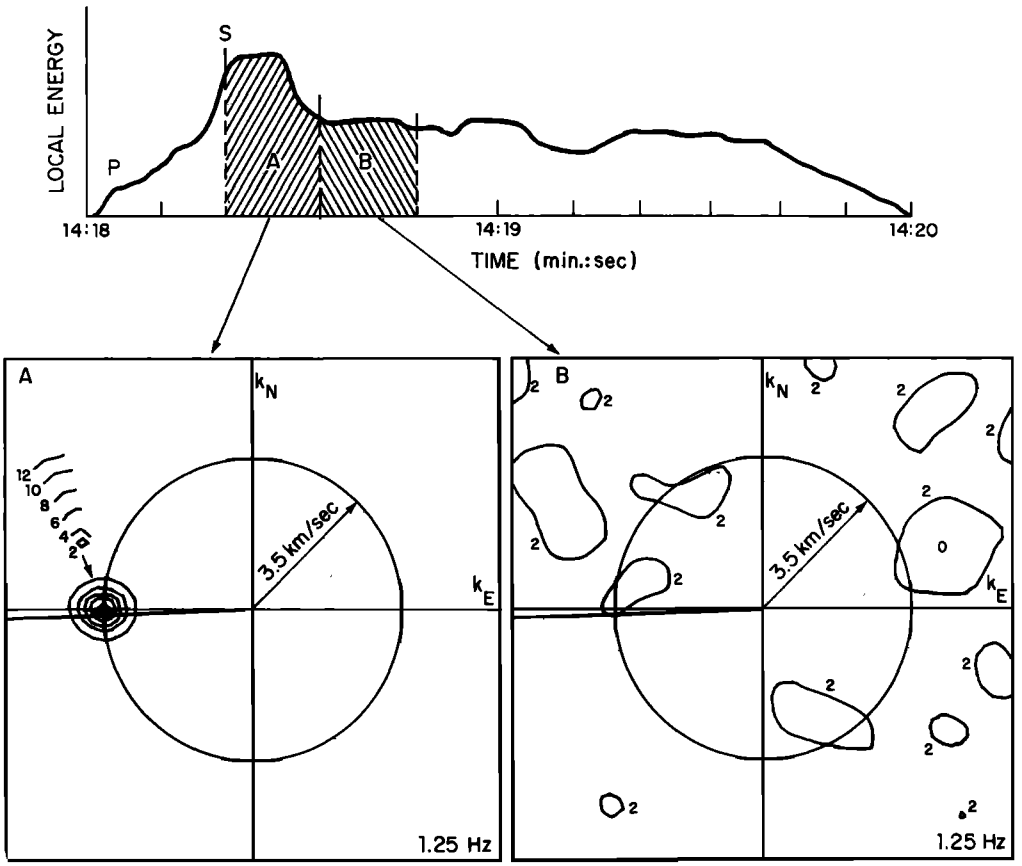

Fig. 2. High-resolution spectra for S arrival and S coda in frequency band 1.0–2.0 Hz for strip-mining blast near Lasa. This figure is reproduced from *Scheimer and Landers* [1974].

quakes. If so, however, it seems rather fortuitous that the time function for the decay of amplitude is independent of earthquake magnitude (item 4). Secondly, as shown in Figures 7, 8, and 9 of this paper, the amplitude decay curve is very regular and repeatable for different earthquakes. We expect a more erratic, variable decay curve if it represents the intensity of aftershocks.

The 'backscattering' model, on the other hand, satisfactorily explains all the observed facts enumerated before. Strong evidence supporting this model can be found in Figure 2 reproduced from *Scheimer and Landers* [1974]. This figure shows the energy in the frequency band 1.0–2.0 Hz of a short-period record at the F2 subarray of Lasa for a strip-mining blast 113 km away as a function of time. The peak energy in this band is due to the arrival of the S wave. The high-resolution wave number spectrum [*Capon*, 1969] for this section of the record indicates that virtually all the energy is arriving from the direction of the blast. The wave number spectrum for the later S coda indicates that energy is arriving from all directions with shear and surface wave velocities.

Let us then follow the waves as they are generated from an earthquake. The duration of the major event at an earthquake source may be measured roughly by the fault length divided by the rupture velocity. Since the fault length for earthquakes with magnitude (M) 6 is about 10 km and the rupture velocity is roughly the shear velocity, we expect that the source duration of earthquakes with $M < 6$ is less than a few seconds. The duration for an $M1$ earthquake is probably a few hundredths of a second.

We shall call the waves which spread outward from the source 'primary waves.' The nature of primary waves observed at a station will depend on the earth's structure along the wave path from source to station. At high frequencies the appearance of primary waves will be quite different for different wave paths.

As the primary waves spread out, secondary waves are generated at each of the heterogeneities that they encounter. Suppose, for simplicity, that both the primary and the secondary waves are of the same kind of wave with velocity v. Then we consider a time interval $(t, t + \Delta t)$ measured from the origin time where Δt is longer than the duration of primary waves. During this time interval the secondary waves arrive from the heterogeneities within the zone sandwiched by two ellipses (for surface waves; ellipsoids for body waves), both with the foci at source and station and with the length of the major axis equal to vt and $v(t + \Delta t)$.

Consider seismograms of an event recorded at two different stations. For the given time interval $(t, t + \Delta t)$ the two elliptical (or ellipsoidal) zones will increasingly overlap as t increases. Besides, a greater number of heterogeneities will contribute to the later time interval and tend to average out the difference between backscattering energies received at the two stations. Thus the difference in the appearance of seismograms disappears in the coda.

The field of the backscattered waves will appear locally stationary in space and time, implying an equal energy flow in opposite directions across a geologic boundary. Thus the particle velocity in a low-impedance medium will be greater than that in a high-impedance medium when the two are in contact. Since the ambient noise is also stationary, we expect the same amplification effect for a low-impedance medium. Since the ratio of coda amplitude to the ambient noise determines the

tail end of a seismogram, the total duration will not depend on the local geology of the station site.

We shall now summarize the properties of coda waves discussed in this section in the following simple equation for the power spectrum of coda waves at time t measured from the earthquake origin time:

$$P(\omega|t) = S(\omega)C(\omega|t) \tag{1}$$

Here $C(\omega|t)$ is independent of the earthquake source parameters. It represents the effect of a large area and is independent of the distance or the nature of the direct wave path from the source to the station. For a fixed ω, $C(\omega|t)$ depends only on the time t. On the other hand, $S(\omega)$ expresses the effect of earthquake source. Let $P_1(\omega|t)$ and $P_2(\omega|t)$ be the coda power for two different earthquakes. Since $C(\omega|t)$ is common to both and is independent of locations of station or epicenter, we can write

$$\frac{P_1(\omega|t)}{P_2(\omega|t)} = \frac{S_1(\omega)}{S_2(\omega)} \tag{2}$$

Thus the coda power will give us the ratio of source factor $S(\omega)$ for different earthquakes without knowing what $C(\omega|t)$ is. The ratio $S_1(\omega)/S_2(\omega)$ physically means the ratio of total seismic energy generated by an earthquake in the unit frequency band around ω.

Strictly speaking, the assumption that $C(\omega|t)$ is common to all sources implies that different seismic sources share a common composition of wave types, so that the same backscattering effect applies to all. Another implicit assumption is that the duration of primary waves is short in comparison with the time interval Δt over which the coda power $P(\omega|t)$ is estimated. It is also implicit that the spatial dimension of primary source (earthquake) is small in comparison with $v\Delta t$, where v is the velocity of wave propagation. Some of these assumptions may seem to be oversimplifications, but they give results roughly agreeing with observations.

Two Extreme Models of Coda Waves

For a more quantitative exposition of coda wave origin we shall consider two specific models. One is the single-scattering model, in which we consider the coda as a superposition of backscattering wavelets from discrete scattering sources. Each wavelet is due to a single scatterer in the absence of the other scatterers. In this model the scattering is a weak process, and use is made of the Born approximation in that the loss of energy from the primary waves as well as the multiple scattering is neglected. Because of these oversimplifications the law of energy conservation is violated.

In the second model we shall go to the other extreme and consider the seismic energy transfer as a diffusion process. In this case the energy, of course, is conserved. However, the interpretation of the diffusion coefficient in terms of the heterogeneous wave medium is not straightforward.

Let us first consider the single-scattering model and, for simplicity, put the seismic station at the same place as the earthquake source. Let $\phi(\omega|r)$ be the Fourier transform of displacement due to a backscattering wavelet from a single scatterer located at a distance r; $\phi(\omega|r)$ depends on the earthquake source as well as on the scatterer. Assume that the scatterers responsible for coda waves are distributed randomly but uniformly in space, and let $N(r)$ be the number of scattering sources within radius r of the station. Then the number of scatterers in the zone bounded by $(r, r + \Delta r)$ will be $(dN/dr)\,\Delta r$. On the assumption that both primary waves and scattered waves are of the same kind and share the same propagation velocity, the backscattering waves from scatterers in $(r, r + \Delta r)$ will arrive at the station in the time interval $(t, t + \Delta t)$, where $t = 2r/v$ and $\Delta t = 2\Delta r/v$. For a distance range Δr long enough, so that the corresponding Δt is greater than the duration of an individual backscattering wavelet, and for a random distribution of scatterers, the sum of the energy carried by backscattered waves arriving in $(t, t + \Delta t)$ will be equal to Δt times the power spectral density $P(\omega|t)$ of the coda waves. Thus we write

$$P(\omega|t)\Delta t = \sum_{r<r_n<r+\Delta r} |\phi_n(\omega)|^2 = \frac{dN}{dr}\,\Delta r\,|\phi(\omega|r)|^2 \tag{3}$$

where r_n is the distance from the station to the nth scatterer. Let us now consider the scattering of body waves. We assume a density σ of scatterers per unit volume. The number of scatterers within the spherical shell $(r, r + \Delta r)$ is $(dN/dr)\,\Delta r = 4\sigma\pi r^2\Delta r$. From (3) we then write

$$P(\omega|t)\Delta t = |\phi(\omega|r)|^2 4\sigma\pi r^2\Delta r \tag{4}$$

The geometrical spreading being taken into account, the amplitude spectra of the scattered waves will depend on travel distances according to

$$|\phi(\omega \mid r)| = |\phi(\omega \mid r_0)|\left(\frac{r_0}{r}\right)^2 \tag{5}$$

Here r represents the distance between station and scatterer, as well as the distance between the earthquake source and scatterer; r_0 is a reference distance.

In addition to the above geometrical spreading the waves should attenuate due to the anelasticity of the earth medium which turns the seismic energy into heat. By using the quality factor Q the fractional loss of energy per 1 cycle is $2\pi Q^{-1}$, and the attenuation in power during the time period t is exp $\{-\omega t/Q\}$, where ω is the angular frequency. We then write the secondary wave intensity

$$|\phi(\omega \mid r)| = |\phi(\omega \mid r_0)|\left(\frac{r_0}{r}\right)^2 e^{-\omega t/2Q} \tag{6}$$

From (4) and (6) and since $r = vt/2$, $\Delta r = v\Delta t/2$, we obtain the expression for the power spectral density of coda waves as backscattering body waves:

$$P(\omega|t) = |\phi(\omega|r_0)|^2 8r_0^4\pi\sigma v^{-1}t^{-2}e^{-\omega t/Q} \tag{7}$$

On the other hand, if the coda is made of backscattering surface waves, we obtain another formula,

$$P(\omega|t) = |\phi(\omega|r_0)|^2 2r_0^2\pi\sigma t^{-1}e^{-\omega t/Q} \tag{8}$$

where σ is now the density of scatterers per unit area. Both (7) and (8) can be written in a more general form as

$$P(\omega|t) = St^{-m}e^{-\omega t/Q} \tag{9}$$

the constant m being determined by the geometrical spreading, with $m = 1$ for surface waves and $m = 2$ for body waves. The source term S in (9), which varies with earthquake magnitude, represents the effect of both the primary and the secondary wave sources. Since the secondary wave source, namely the scattering by heterogeneity, is common to all earthquakes (as long as the composition of primary waves is the same), the difference in this source factor should be due to the difference in the earthquake source.

Within the scheme of this single-scattering theory, however, we have a serious conceptual difficulty concerning the physical meaning of Q introduced above. Should this Q include the loss

by scattering in addition to the anelastic loss? At first it may look as if the inclusion of loss by scattering is an improvement over the simple single-scattering theory. Then one realizes that the multiple scattering may pump the energy back to the primary waves as well as to the backscattering waves. The basic difficulty comes from the inadequacy of the Born approximation in dealing with the energy balance. It violates the law of conservation of energy [*Howe*, 1971, 1973*a*, *b*].

To avoid the above difficulty, we shall now consider the other extreme model in which all the seismic energy is scattered through diffusion. Such a model has been applied previously to the earth by *Wesley* [1965] and to the moon by *Nakamura et al.* [1970]. Let $E(\mathbf{x}, t, \omega)$ be the seismic energy per unit volume within a unit frequency band around ω. Then the conservation of energy leads to a modified diffusion equation including linear dissipation

$$\frac{\partial E}{\partial t} = D\nabla^2 E - \frac{\omega}{Q} E \tag{10}$$

where D is the diffusivity and the last term represents the loss by anelasticity which turns the seismic energy into heat. Clearly, here Q is the intrinsic quality factor and does not include the loss by scattering.

The solution of (10) for a point source in time and space is given by

$$E(\mathbf{x}, t, \omega) = \frac{W(\omega)}{(4\pi Dt)^{3/2}} \exp\left(-\frac{x^2 + y^2 + z^2}{4Dt}\right) \cdot \exp\left(-\frac{\omega t}{Q}\right) \tag{11}$$

for three-dimensional diffusion corresponding to body wave scattering. Here $W(\omega)$ is the total seismic energy generated by the earthquake within the unit frequency band around ω.

For large t and small distance $(x^2 + y^2 + z^2)^{1/2}$ at which the coda waves are observed, (11) becomes a function of only time t and is independent of distance; this is an observed result for coda power. Since we defined the coda power $P(\omega|t)$ for ground displacement and the seismic energy per unit volume is twice the kinetic energy for propagating waves or stationary vibrations, we have

$$\rho\omega^2 P(\omega|t) = E(0, t, \omega) \tag{12}$$

Putting (11) into (12), we get

$$P(\omega \mid t) = \frac{W(\omega)}{\rho\omega^2(4\pi Dt)^{3/2}} \exp\left(-\frac{\omega t}{Q}\right) \tag{13}$$

Thus the diffusion theory gives a power of t $(-3/2)$ intermediate to body wave (-2) and surface wave (-1) single-scattering theories.

Coming back to (3), we now rewrite the equation for coda power as

$$P(\omega \mid t) = \frac{v}{2}\frac{dN}{dr}\left|\phi\left(\omega\left|\frac{v}{2}t\right.\right)\right|^2 \tag{14}$$

In order to relate this equation with the usual scattering formula we shall formulate the scattering problem following *Chernov* [1960]. Consider a heterogeneous region of volume V buried in an unbounded homogeneous medium. Acoustic plane waves $A_0 e^{i\omega[t-(x/c)]}$ propagating in the x direction are incident on the heterogeneous region. Observations of the scattered waves are made in the far field (Fraunhofer zone) in the homogeneous medium, at which the scatterer volume V may be considered as a point source, so that the scattered waves may be approximated as $A_1 e^{i\omega[t-R/c)]}$, where R is the distance between the center of V and the station. For wavelength λ and linear dimension L of the scatterer volume V, the distance R must be greater than $2L^2/\lambda$ to be in the Fraunhofer zone. Then the scattered power $|A_1|^2$ is proportional to the incident power $|A_0|^2$, the volume V of the heterogeneous region, and the reciprocal R^{-2} of squared distance. Putting the proportionality factor $g(\theta)/4\pi$, where θ is the angle between the direction from the center of scattering volume to the station and the direction of propagation of incident waves (x axis), we have

$$|A_1|^2 = |A_0|^2 \frac{Vg(\theta)}{4\pi R^2} \tag{15}$$

The average of $g(\theta)$ over all directions is equal to the fractional loss of energy by scattering and is called the 'turbidity coefficient.' The value $g(\theta)/4\pi$ is equal to the fractional loss of energy by scattering per unit solid angle around the direction θ.

Coming back to our problem of coda waves, we shall put the Fourier transform of primary waves at the distance r to be $\phi_0(\omega|r)$. For large r the incident waves may be considered to be plane waves locally. Consider, then, the incident plane waves $A_0 = \phi_0(\omega|r)$ upon the heterogeneous region of volume $V = 4\pi r^2 \Delta r$. If there is only one scatterer in the volume V, $A_1 = \phi(\omega \mid r)$. Since there are $(dN/dr)\,\Delta r$ scatterers in V and they add randomly, we have the relation $|A_1|^2 = (dN/dr)\,\Delta r|\phi(\omega|r)|^2$. Putting these relations into (15), we have

$$\frac{dN}{dr}|\phi(\omega \mid r)|^2 = g(\pi)|\phi_0(\omega \mid r)|^2 \tag{16}$$

where we put $\theta = \pi$, assuming a literal backscattering. The value $g(\pi)$ is 4π times the fractional loss of energy by scattering in the backward direction per unit solid angle. We shall call $g(\pi)$ the 'backward turbidity coefficient.' Putting (16) into (14), we have a remarkably simple formula for coda power spectrum:

$$P(\omega \mid t) = \frac{v}{2} g(\pi)\left|\phi_0\left(\omega\left|\frac{vt}{2}\right.\right)\right|^2 \tag{17}$$

The above equation relates the observed coda power with the spectrum of primary waves. If both are known, we can find the backward turbidity coefficient which will give some constraint on the nature of heterogeneity.

For an acoustic random medium characterized by the mean square fluctuation $\langle\mu^2\rangle$ of the refractive index and spatial autocorrelation function $N(r) = e^{-r/a}$, *Chernov* [1960] gives the following formula for $g(\theta)$:

$$g(\theta) = \frac{8k^4a^3\langle\mu^2\rangle}{\left(1 + 4k^2a^2\sin^2\frac{\theta}{2}\right)^2} \tag{18}$$

where k is the wave number $2\pi/\lambda$. Chernov also gives the following result for $N(r) = e^{-r^2/a^2}$:

$$g(\theta) = (\pi)^{1/2}k^4a^3\langle\mu^2\rangle \exp\left(-k^2a^2\sin^2\frac{\theta}{2}\right) \tag{19}$$

It is interesting to note that the above two different $N(r)$ give similar results for forward scattering ($\theta \simeq 0$) for any ka but give drastically different results for backscattering ($\theta \simeq \pi$) for large ka. For example, *Aki* [1973] fitted the Chernov model to the scattering of P waves with frequency 0.5 Hz under the Montana Lasa, with parameters $ka = 5$, $\langle\mu^2\rangle = 0.0016$, and $a =$

10 km, which give the backward turbidity coefficients 8×10^{-5} per kilometer for $N(r) = e^{-r/a}$ and 2.5×10^{-12} per kilometer for $N(r) = e^{-r^2/a^2}$. At frequencies higher than 0.5 Hz the backward turbidity coefficients stay nearly the same for $N(r) = e^{-r/a}$ but become smaller for $N(r) = e^{-r^2/a^2}$.

Similarly, in our diffusion model the diffusivity D may be related to the wave-scattering process. In analogy with the scattering of particles moving with a certain mean free path, *Dainty et al.* [1974*b*] obtained the relation between D and the mean free path l as

$$D = \frac{vl}{3} \tag{20}$$

where v is the velocity of wave propagation and l is defined as the distance travelled by the primary wave, over which its energy is reduced to e^{-1} by scattering. By definition, l is the reciprocal of the turbidity coefficient. Since the scattered energy in the forward direction behaves more like waves rather than a diffusion process, the diffusion theory may apply only to the part of energy scattered in the backward direction. Then the turbidity coefficient which enters in (20) through l should probably be the backward turbidity $g(\pi)$ rather than the average of $g(\theta)$ over all directions. Thus we get two rough estimates of backward turbidity, one by the single-scattering theory and the other by the diffusion theory.

At this point one may question the relevance of the solution (13) of the diffusion equation for a point source to our problem, if the diffusion theory applies to the part of the energy scattered in the backward direction. It may be more appropriate to assume a scattering source moving with the primary waves.

In a later section we shall make a rough estimate of diffusivity by using (13). We shall find that the diffusivity is rather high, $10^{12} \sim 10^{13}$ cm^2/s. For the range of time 20–200 s, at which most coda measurements were made, the above diffusivity gives the mean diffusion distance greater than or comparable to the travel distance of primary waves.

It appears, then, that as the primary waves spread out, they will leave behind a pool of scattered energy which becomes quickly homogeneous inside the pool because of high diffusivity. Then the coda amplitude decay observed in the pool will depend on the rate of energy pumped into the pool, the rate of increase in volume of the pool, and the rate of intrinsic loss of energy (conversion to heat). The rate of energy pumped into the pool depends on the amplitude history of primary waves, which not only lose energy by scattering but also gain energy back from the pool by diffusion. This is a complex process and cannot be rigorously treated by our rudimentary theory. The approach from the kinetic theory for wave propagation in random medium, such as that discussed by *Howe* [1973*b*], may be promising but is beyond the scope of this paper. We feel, however, that the validity of (9) may survive a more rigorous treatment.

Analysis of Data

The earthquakes selected for the present study were recorded on a spectral analyzing seismograph designed and constructed by M. Tsujiura of Tokyo University. Tsujiura's instruments have been operated at several places in Japan and other countries. One of them was recently operated for a year at the Stone Canyon Observatory of the U.S. Geological Survey, near Hollister, California. The seismograph consists of one transducer, an amplifier, a low-pass filter with the corner frequency of 1 Hz, and five band-pass channel filters with

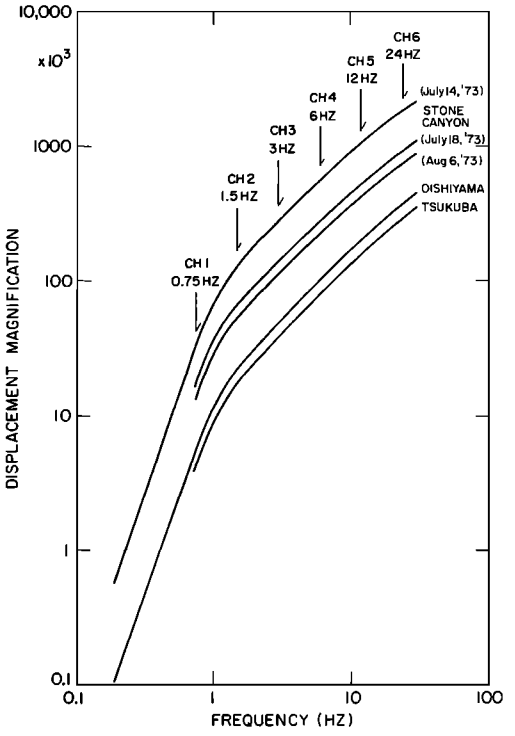

Fig. 3. Seismometer-amplifier frequency response for the different regions studied. The seismometer has a natural frequency of 1 Hz and a damping factor of 0.8.

center frequencies at 1.5, 3, 6, 12, and 24 Hz and respective bandwidths of 1, 2, 4, 8, and 16 Hz. The amplifier and filter responses are shown in Figures 3 and 4. The output of the six filters is recorded continuously on an ink-writing 6-channel recorder. Examples of records of coda amplitudes obtained at Stone Canyon are shown in Figure 5 for three earthquakes with magnitudes M_L of 1.0, 2.1, and 2.9. These events occurred within about 15 km from the observatory. Similar records were obtained for events in Japan, as shown in Figure 6 for two earthquakes, A (M = 3.5) and B (M = 4.8), near Tsukuba. The amplitude decay curve of the coda shown in Figures 5 and 6 is very regular. It is also reproducible for many earthquakes of different magnitudes at various frequencies, as is illustrated by Figures 7, 8, and 9. We analyzed about 200 earthquakes with magnitudes between 1 and 5.5 in Japan and California. Most of these events occurred within about 50 km of Tsukuba (36°12'39"N, 140°06'35"E) or Oishiyama (34°05'56"N,

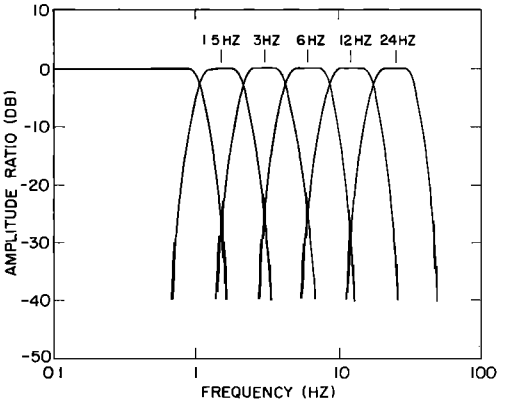

Fig. 4. Frequency response of low-pass and band-pass filters used in the spectral analysis.

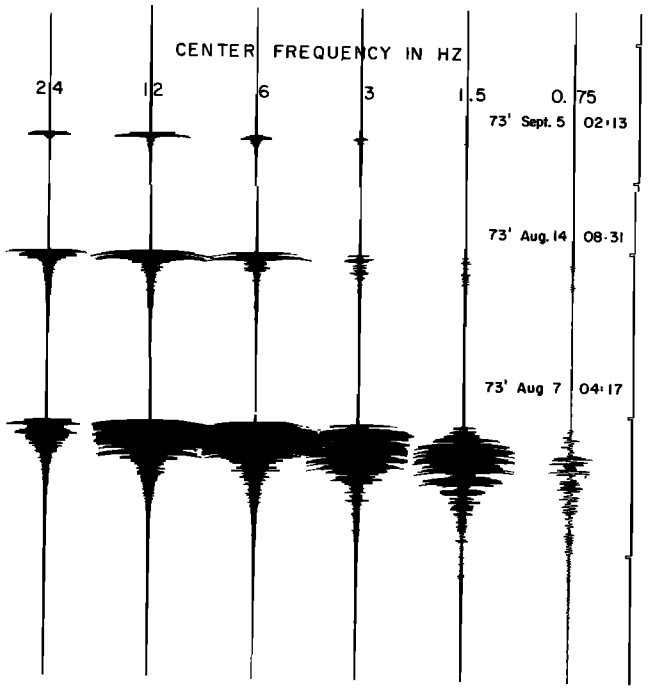

Fig. 5. Traces of three events with magnitudes 1 (top), 2.1 (middle), and 2.9 (bottom) recorded at Stone Canyon, California, with the spectral analyzing seismograph. Channel center frequencies are indicated at the top of the figure. Tick marks on right side of figure are minute marks.

135°19'00"E), Japan, or Stone Canyon (36°38'12"N, 121°15'18"W), California. The focal depths of earthquakes near Tsukuba (Figure 10) ranged from 40 to 90 km. The earthquakes recorded at Oishiyama (Figure 11) were generally shallower than 10 km, with a few deeper shocks between 20 and 50 km. The focal depths of all the earthquakes recorded at Stone Canyon (Figure 12) were shallower than 15 km. Recording covered the periods of December 1969 to August 1971 at Tsukuba, July 1970 to December 1971 at Oishiyama, and July to September 1973 and January to February 1974 at Stone Canyon. A list of events used in this study is given in Tables 1, 2, and 3.

The envelopes of the peak to peak coda amplitudes, smoothed manually, were measured from the chart records by using an x-y digitizer. Samples were taken every 2 s for small events lasting less than 150 s after origin time and every 4 s for larger events. Noise levels were compared before and after each event on all channels, and corrections were applied when it was necessary. The beginning of the digital recording of coda amplitudes was arbitrarily chosen at a point in the seismogram where the seismic signal started to decay in a regular manner.

As is well-known, the Fourier transform of a power spectrum is the autocorrelation function

$$\phi(\tau) = \langle f(t)f(t+\tau)\rangle = \frac{1}{2\pi}\int_{-\infty}^{\infty} P(\omega \mid t)e^{i\omega\tau}\,d\omega \qquad (21)$$

For zero lag the autocorrelation function is the mean square of the time series

$$\phi(O) = \langle f^2(t)\rangle \qquad (22)$$

In our case of transient time series the mean square may be estimated from a short time sample around a given absolute time. We now write

$$\langle f^2(t)\rangle = \frac{1}{2\pi}\int_{-\infty}^{\infty} P(\omega \mid t)\,d\omega \qquad (23)$$

Then for a band-passed signal with $P(\omega|t) = P$ (constant) for $\omega_0 < |\omega| < \omega_1$ and $P(\omega|t) = 0$ otherwise, we have

$$\langle f^2(t)\rangle = 2P\Delta f \qquad (24)$$

where $\Delta f = (\omega_1 - \omega_0)/2\pi$.

Thus for a rough approximation the mean square amplitude is equal to the product of the power spectral density and the bandwidth. Since our manually smoothed peak to peak amplitude, $A(\omega|t)$, corresponds to roughly twice the rms value of the signal, we write

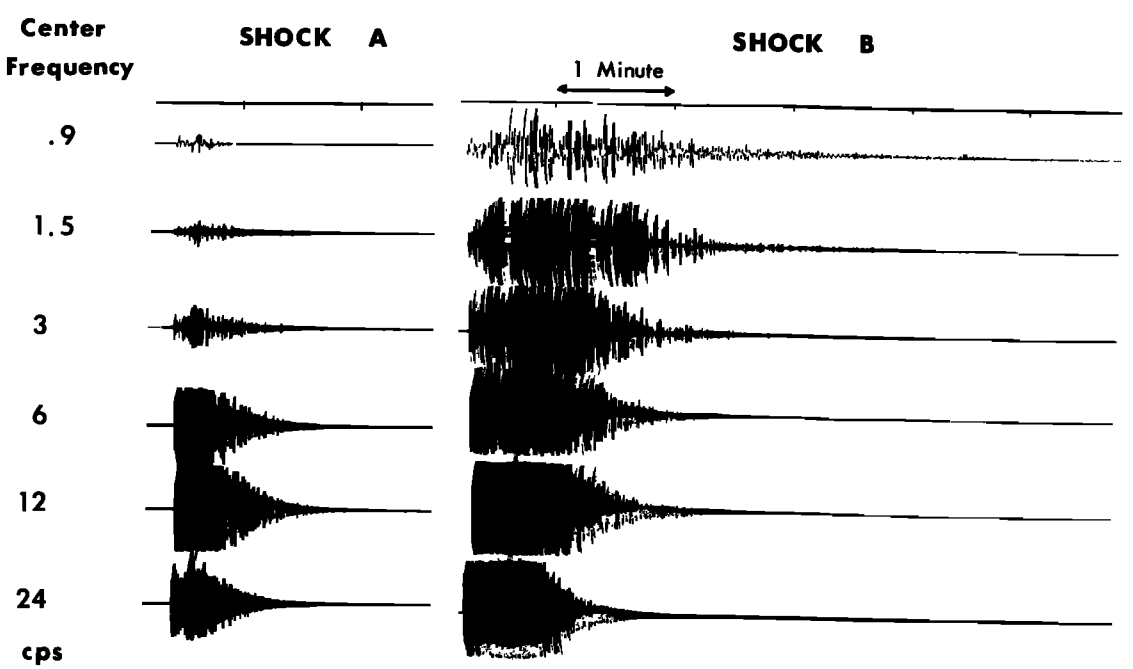

Fig. 6. Traces of two events, A (M = 3.5) and B (M = 4.8), recorded at Tsukuba, Japan, with the spectral analyzing seismograph. Channel center frequencies are indicated at left. Tick marks on top are minute marks.

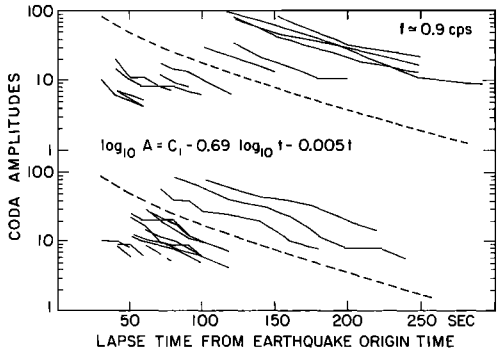

Fig. 7. Amplitude decay traces of coda waves measured at 0.9 Hz from earthquakes near Tsukuba, Japan. The dashed lines represent the function $\log_{10} A = C_i - 0.69 \log_{10} t - 0.005t$ obtained by fitting a standard decay curve to this ensemble of traces (see text for explanation of symbols and procedure).

$$A(\omega|t) = 2[2P(\omega|t)\Delta f]^{1/2} \tag{25}$$

where Δf is the bandwidth of the filter on the particular channel considered and $P(\omega|t)$ is the coda power defined previously. Inserting (25) into (17), we obtain the formula for the amplitude of coda with angular frequency ω at a time t:

$$A(\omega \mid t) = 2\left|\phi_0\left(\omega\left|\frac{vt}{2}\right.\right)\right| [g(\pi)]^{1/2}(v\Delta f)^{1/2} \tag{26}$$

As is discussed in the preceding section either for the single scattering theory or for the diffusion theory, the coda amplitude $A(\omega|t)$ will take the following simple form as a function of time measured from the origin time:

$$A(\omega|t) = ct^{-a}e^{-\omega t/2Q} \tag{27}$$

where c represents the coda source factor at the particular frequency ω, a is a constant that depends on the geometrical spreading, and Q is the quality factor (from (9) and (25), $c = 2(2\Delta f S)^{1/2}$ and $a = m/2$).

Taking the logarithm of both sides in formula (27), we obtain

$$\log_{10} A(\omega|t) = C - a \log_{10} t - bt \tag{28}$$

where $C = \log_{10} c$ and b is related to the quality factor Q by the relation

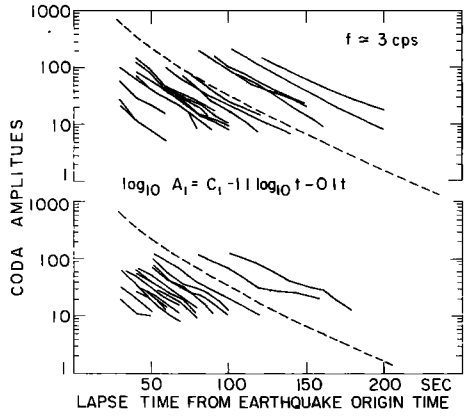

Fig. 8. Amplitude decay traces of coda waves at 3 Hz from earthquakes near Tsukuba, Japan. The dashed lines represent the function $\log_{10} A = C_i - 1.1 \log_{10} t - 0.1t$ obtained by fitting a standard decay curve to this ensemble of traces (see text for explanation of procedure).

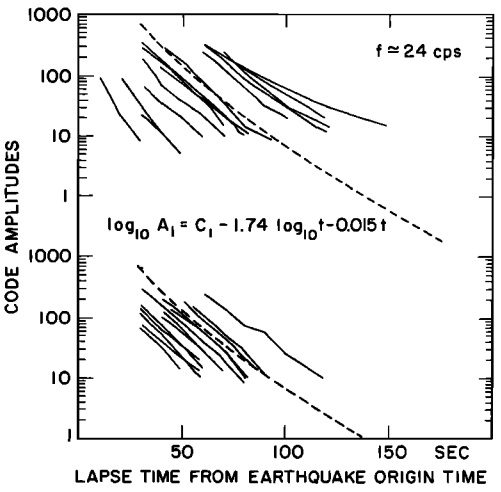

Fig. 9. Amplitude decay traces of coda waves at 24 Hz from earthquakes near Tsukuba, Japan. The dashed lines represent the function $\log_{10} A = C_i - 1.74 \log_{10} t - 0.015t$ obtained by fitting a standard decay curve to this ensemble of traces (see text for explanation of procedure). The extent of coda duration at this frequency is of special interest.

$$b = (\log_{10} e)\frac{\pi f}{Q} \tag{29}$$

The effects of source factor, geometrical spreading, and attenuation were separated out by the method of least squares. Each channel filter output was treated separately, and fits were obtained with the formula (28) by considering simultaneously all the events of an ensemble of earthquakes recorded on a given channel. In solving the least squares problem, provisions were made in the computation for different choices of the spreading factor a: a = free, $a = 0.5$, or $a = 1$.

The coda source factors C calculated at Tsukuba, Stone Canyon, and Oishiyama are shown plotted against frequency in Figures 13 and 14. The frequency dependences of C obtained in Japan and California are quite different. At Tsukuba they are rather flat in the frequency range of 1–24 Hz and somewhat richer in high frequencies in region A than in region C (see

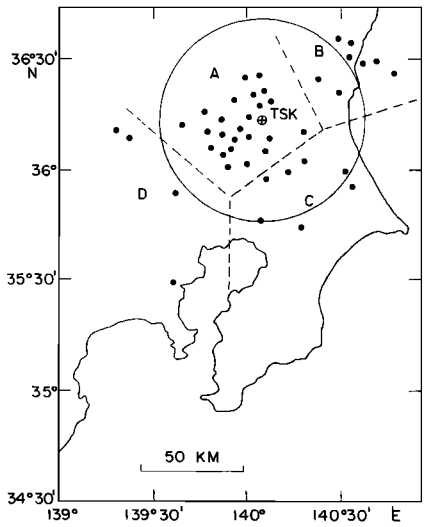

Fig. 10. Epicenters of earthquakes near Tsukuba (TSK), Japan, used in the coda analysis. Most epicenters are within a radius of 50 km from the station. Hypocentral depths vary from 20 to 90 km. A list of these events is given in Table 3.

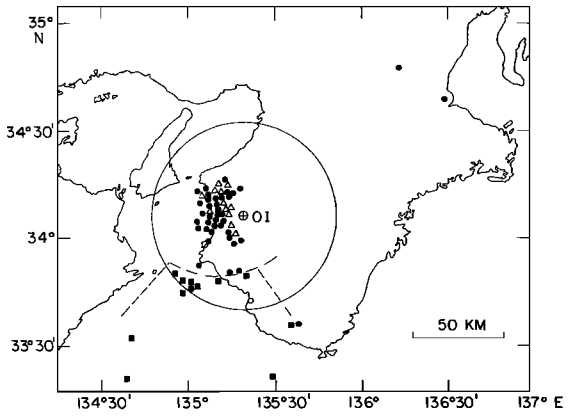

Fig. 11. Epicenters of earthquakes near Oishiyama (OI), Japan, used in the coda analysis. A list of these events is given in Table 2. Triangles and closed circles refer to the first two series of events studied, characterized by focal depths shallower than 15 km. Closed squares, within the area outlined by dashed lines, refer to the third series of events with deeper focus (25 < depth < 50 km). Most epicenters are within a radius of 50 km from the station.

Figure 10). Similar results are obtained for Oishiyama in the frequency range of 1–12 Hz. There is no marked effect of depth on the spectra of earthquakes in this region. For Oishiyama the spectral shape of the coda source factor does not change even with the earthquake magnitude. On the other hand, we observe a strong scale effect on the spectral shape at Stone Canyon. With increasing earthquake magnitudes the rate of increase in the coda source factors at 24 Hz is much slower than at 1 Hz.

Computed residuals show that the coda amplitudes can be expressed by formula (28) within errors of 10–20%. As shown in Figures 7, 8, and 9 the decay of coda amplitudes at Tsukuba is very regular and reproducible for many different events. This observation, along with similar observations made at Oishiyama and Stone Canyon, supports our assumption that both factors a and b are independent of the location of epicenter and the magnitude of the earthquake. The values computed for the factor a (Table 4), however, are very sensitive to the coda amplitude for small t. Because of the clipping introduced on some of the recorded events the amplitude in the early coda is not always well-defined. This fact and the inherent difficulty to define exactly when the coda starts explain the erratic behavior of this coefficient when it is estimated from the data. Fortunately, the estimate for b (Tables 5*a*, 5*b*, 5*c*) is insensitive to the uncertainty in the estimate of a because $a \log t$, although it varies strongly for small t, varies much less than bt over most of the coda length. In what follows we shall then restrict our attention to the results derived from the coefficient b.

Regional Seismic Attenuation Properties of the Earth's Crust

From (29) and through the use of the estimated values of b obtained from the least squares fits (Tables 5*a*, 5*b*, and 5*c*) a value of the quality factor was calculated at each channel filter frequency. The estimates of Q represent an average value over the region encompassed by the coda waves from many different local earthquakes. In Figure 15 the values of Q^{-1} determined at Tsukuba, Japan, and Stone Canyon, California, are shown plotted against frequency for the various choices of the spreading factor a. As we pointed out earlier, because of the particular form of (28), the uncertainty associated with the parameter a has very little effect on the result derived for Q. In both regions displayed, Q increases with frequency independent of the choice of a and merges to the value of about 1000 at 20 Hz. At 1 Hz, however, Q is low and quite variable between the two regions ($Q \simeq 70$ at Stone Canyon and $Q \simeq 200$ at Tsukuba).

The results obtained for Q for different groups of events at Tsukuba, Oishiyama, and Stone Canyon are summarized in Figure 16. In this analysis the factor a was fixed to 1. The numbers attached to the different regions refer to the groups of events shown in Tables 5*a*, 5*b*, and 5*c*. The quality factor again shows consistently low values at 1 Hz that are quite variable among regions. On the assumption now that these values were to be applicable at 24 Hz also, one would expect the coda within the corresponding frequency band to die off in a matter of a few seconds. Figure 9, however, clearly shows that it can last for 100 s or more at this frequency. Thus the Q of coda waves must increase with frequency. This does not necessarily mean that the Q of crustal material is frequency dependent. We may be observing the dependence of Q on depth for waves scattered from different parts of the earth's crust. In other words, this apparent frequency dependence can be explained if the coda waves at 1 Hz are primarily composed of surface waves scattered from shallow heterogeneities and those at 24 Hz are primarily backscattering body waves from the deep, high-Q lithosphere. The low values of Q obtained near 1 Hz are consistent with the Q determined by other workers using direct waves from shallow earthquakes near 10 Hz [*Clowes and Kanasewich*, 1970; *O'Neill and Healy*, 1973]. On the other hand, the high Q of about 1000 at 20 Hz is consistent with the results reported by *Clowes and Kanasewich* [1970] for the lower crust and with the Q value of the lithosphere obtained from surface wave attenuation [*Tsai and Aki*, 1969].

Earthquake Source Spectrum

The source factor of coda amplitude is proportional to the square root of total seismic energy within a unit frequency band around ω (equation (13)) or equivalently to the absolute value of the Fourier transform of primary waves at a reference distance in the far field (equation (26)). Then the relative values of the source spectrum for two different earthquakes can be determined from the ratio of the source factor of coda amplitude. In order to fix their absolute values, however, one

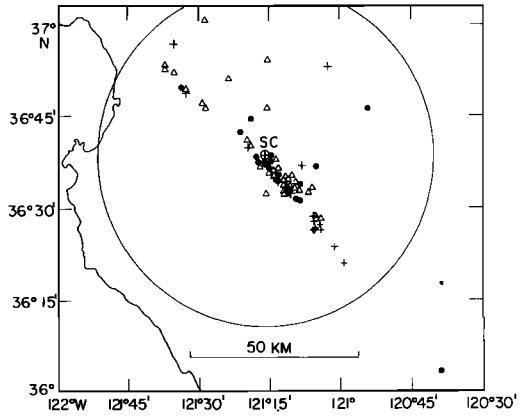

Fig. 12. Epicenters of earthquakes near Stone Canyon (SC), California, used in the coda analysis. A list of these earthquakes is given in Table 1. Triangles refer to the first series of events studied, closed circles and crosses, to series 2 and 3, respectively. All the earthquakes in this area are shallower than 15 km and are mostly confined within 50 km of the station.

TABLE 1. Events Recorded at Stone Canyon (36°38'12"N, 121°15'18"W)

Event	Date	Origin Time, UT	North Latitude	West Longitude	Depth, km	Magnitude
			Series 1: 1973			
1	July 17	16h 48m 51.5s	36°32.1'	121°06.3'	12.0	1.9
2	July 18	05h 55m 15.4s	36°45.8'	121°15.2'	11.4	1.6
3	July 18	08h 23m 37.9s	36°33.6'	121°11.5'	8.1	2.8
4	July 18	22h 52m 47.9s	36°33.6'	121°11.5'	7.7	1.5
5	July 19	14h 53m 03.1s	36°33.0'	121°05.8'	11.9	1.8
6	July 19	20h 06m 00.1s	36°34.3'	121°12.2'	7.3	2.0
7	July 20	15h 54m 26.6s	36°33.5'	121°11.4'	7.8	1.5
8	July 21	09h 36m 48.8s	36°37.6'	121°16.2'	5.6	2.0
9	July 21	09h 57m 11.0s	36°37.6'	121°16.2'	5.5	2.3
10	July 21	11h 45m 35.0s	36°31.6'	121°08.7'	5.1	2.3
11	July 21	14h 20m 26.3s	36°37.8'	121°16.4'	4.1	1.9
12	July 23	13h 54m 02.0s	36°36.9'	121°15.4'	6.0	2.1
13	July 23	21h 29m 05.4s	36°27.9'	121°05.1'	9.0	2.2
14	July 24	22h 55m 00.8s	36°35.1'	121°13.8'	8.2	1.7
15	July 26	01h 31m 59.4s	36°45.8'	121°28.4'	5.6	2.4
16	July 26	17h 21m 28.2s	36°32.4'	121°09.5'	4.9	2.2
17	Aug. 1	02h 30m 20.5s	36°39.9'	121°19.5'	5.5	2.0
18	Aug. 2	04h 26m 35.8s	36°52.9'	121°37.3'	5.7	3.0
19	Aug. 2	05h 44m 44.5s	36°52.8'	121°37.3'	5.6	3.1
20	Aug. 2	07h 53m 01.9s	36°37.1'	121°16.6'	9.8	2.0
21	Aug. 2	16h 10m 42.3s	36°32.7'	121°10.5'	7.9	3.3
22	Aug. 3	02h 18m 45.3s	36°50.6'	121°24.2'	9.4	2.5
23	Aug. 4	05h 20m 38.2s	36°35.8'	121°13.7'	4.5	1.5
24	Aug. 5	16h 56m48.7s	36°33.0'	121°10.5'	6.0	2.8
25	Aug. 5	17h 09m11.5s	36°32.9'	121°10.6'	6.1	2.0
26	Aug. 5	20h 45m 38.5s	36°32.9'	121°10.5'	6.8	2.0
27	Aug. 6	05h 57m 43.2s	36°36.5'	121°14.8'	5.1	2.1
28	Aug. 7	04h 17m 01.1s	36°46.8'	121°29.3'	4.9	2.9
29	Aug. 8	15h 51m 05.5s	36°40.5'	121°20.0'	4.3	1.8
30	Aug. 10	11h 35m07.7s	36°35.9'	121°13.5'	3.7	3.1
31	Aug. 10	11h 51m 01.8s	37°03.2'	121°29.0'	6.2	2.8
32	Aug. 14	08h 31m 01.1s	36°34.1'	121°11.9'	6.2	2.1
33	Aug. 15	00h 36m 48.5s	36°53.9'	121°15.6'	5.3	2.6
34	Aug. 17	16h 41m 48.3s	36°35.4'	121°13.8'	7.5	2.5
35	Aug. 19	00h 05m 09.0s	36°33.8'	121°11.6'	6.3	2.3
36	Aug. 20	07h 33m 23.1s	36°32.7'	121°10.8'	7.7	2.6
37	Aug. 20	12h 48m 34.2s	36°32.9'	121°10.6'	7.7	1.8
38	Aug. 20	17h 35m 14.2s	36°34.6'	121°12.6'	7.7	2.2
39	Aug. 21	09h 29m 39.0s	36°49.1'	121°33.1'	6.1	2.9
40	Aug. 23	10h 57m 47.6s	36°33.8'	121°11.4'	3.7	2.1
41	Aug. 23	14h 39m 38.4s	36°27.5'	121°04.3'	9.0	2.3
42	Aug. 26	07h 34m 59.8s	36°51.7'	121°35.3'	5.7	3.0
			Series 2: 1973			
1	Aug. 31	09h 10m 32.9s	36°49.6'	121°33.8'	5.9	2.8
2	Sept. 2	04h 54m 08.6s	36°36.9'	121°14.9'	4.0	1.9
3	Sept. 2	17h 18m 31.0s	36°42.3'	121°21.3'	1.9	2.2
4	Sept. 3	03h 28m 29.5s	36°34.2'	121°12.6'	7.4	1.9
5	Sept. 3	19h 39m 30.1s	36°36.9'	121°15.1'	4.0	2.0
6	Sept. 3	22h 52m 25.7s	36°37.2'	121°15.9'	4.7	1.8
7	Sept. 5	00h 22m 23.0s	36°45.9'	120°54.4'	4.1	1.9
8	Sept. 5	02h 13m 39.9s	36°37.9'	121°15.9'	4.0	1.0
9	Sept. 7	02h 30m 48.4s	36°37.5'	121°16.4'	4.0	1.1
10	Sept. 8	15h 15m 09.6s	35°44.3'	121°19.2'	6.8	2.9
11	Sept. 8	21h 09m 56.0s	36°36.3'	121°05.2'	14.5	1.8
12	Sept. 8	21h 20m 36.5s	36°03.1'	120°39.1'	3.5	2.9
13	Sept. 8	22h 08m 55.3s	36°36.7'	121°14.9'	4.6	1.0
14	Sept. 9	14h 12m 49.3s	36°38.2'	121°15.0'	7.0	1.0
15	Sept. 9	16h 08m 07.9s	36°38.1'	121°17.3'	6.9	1.3
16	Sept. 11	03h 35m 31.8s	36°31.0'	121°08.5'	9.2	2.1
17	Sept. 11	03h 38m 23.6s	36°31.0'	121°08.6'	9.6	2.0
18	Sept. 11	05h 07m 51.5s	36°33.5'	121°09.1'	6.4	2.1
19	Sept. 11	19h 11m 21.9s	36°35.0'	121°13.6'	6.7	1.0
			Series 3: 1974			
1	Jan. 10	10h 55m 41.5s	36°37.4'	121°08.6'	15.5	2.0
2	Jan. 13	00h 31m 11.5s	36°27.0'	121°04.6'	6.9	2.2
3	Jan. 13	11h 31m 57.7s	36°29.2'	121°05.8'	1.5	2.1
4	Jan. 13	22h 49m 10.1s	36°57.2'	121°35.7'	7.3	2.6
5	Jan. 14	05h 38m 26.6s	36°32.5'	121°11.0'	7.4	2.2
6	Jan. 14	06h 56m 34.1s	36°32.6'	121°11.1'	7.3	2.3
7	Jan. 14	23h 25m 41.1s	36°28.6'	121°06.1'	4.8	2.2
8	Jan. 16	11h 54m 18.4s	36°24.1'	121°01.7'	7.4	2.2

Table 1. (continued)

Event	Date	Origin Time, UT	North Latitude	West Longitude	Depth, km	Magnitude
9	Jan. 16	15h 32m 59.6s	36°32.7′	121°11.1′	7.0	1.9
10	Jan. 16	16h 15m 22.2s	36°53.2′	121°02.8′	1.0	1.9
11	Jan. 16	22h 26m 43.6s	36°33.0′	121°11.8′	7.1	1.9
12	Jan. 18	04h 24m 17.6s	36°21.5′	120°59.0′	11.6	2.1
13	Jan. 22	00h 05m 15.3s	36°39.8′	121°19.7′	5.2	2.0
14	Jan. 23	01h 37m 58.5s	36°22.0′	120°25.5′	12.0	3.2
15*						
16*						
17	Jan. 26	00h 12m 58.6s	36°27.7′	121°04.7′	2.2	2.2
18	Jan. 26	12h 53m 46.7s	36°48.4′	121°32.5′	7.0	2.1
19	Jan. 27	19h 22m 13.7s	36°35.3′	121°14.0′	6.9	2.7
20	Jan. 28	22h 40m 12.2s	36°27.1′	121°05.1′	8.5	2.3
21	Jan. 30	05h 54m 40.3s	36°27.2′	121°05.0′	7.1	2.2
22	Feb. 5	04h 19m 51.2s	36°32.9′	121°10.9′	7.1	1.9
23	Feb. 7	06h 54m 42.0s	36°27.3′	121°04.9′	8.7	2.4
24	Feb. 7	10h 35m 05.9s	36°34.4′	121°12.5′	5.0	3.2

* Events for which precise origin time is not available.

must apply more direct methods to at least one of the earthquakes. We shall apply the far field solution of an infinitesimal dislocation buried in an infinite medium [e.g., *Maruyama*, 1963] to the smallest and closest earthquakes for which the distance to the station is short enough for scattering to be negligible and long enough to be in the far field.

Some of the records of these smallest and closest earthquakes obtained by the Tsujiura band-pass filter seismograph are shown for Stone Canyon and Oishiyama in Figure 17. They show simple P and S wavelets, suggesting the validity of applying the simple far field solution outlined above. We cannot find such simple records for Tsukuba because the nearest earthquakes there are more than 40 km away, which is too far.

Consider a point dislocation source with the seismic moment having the Fourier transform $M(\omega)$. Then the Fourier transform $F(\omega)$ of displacement due to far field P waves in an unbounded homogeneous elastic medium at a distance r from the source can be written as

$$|F(\omega)| = c(4\pi\rho\alpha^3 r)^{-1}|\dot{M}(\omega)| \tag{30}$$

where c is a geometrical factor equal to or less than 1, α is the velocity of P waves, and $\dot{M}(\omega)$ is the Fourier transform of the time derivative of seismic moment. For a band-passed signal with $|F(\omega)| = F$ (constant) in $\omega_0 < |\omega| < \omega_1$, $|F(\omega)| = 0$ otherwise, and $\phi(\omega) = 0$ for all ω, the corresponding signal $f(t)$ is written as

$$f(t) = \frac{1}{2\pi}\int_{-\omega_1}^{-\omega_0} Fe^{i\omega t}\,d\omega + \frac{1}{2\pi}\int_{\omega_0}^{\omega_1} Fe^{i\omega t}\,d\omega$$

$$= 2Ff_1\frac{\sin\omega_1 t}{\omega_1 t} - 2Ff_0\frac{\sin\omega_0 t}{\omega_0 t} \tag{31}$$

where $f_0 = \omega_0/2\pi$ and $f_1 = \omega_1/2\pi$. The maximum amplitude is at $t = 0$ and is equal to

$$f(0) = 2F(f_1 - f_0) = 2F\Delta f \tag{32}$$

Thus for a rough approximation the amplitude of a wavelet is the product of its amplitude spectral density and twice the bandwidth. From known bandwidth of the band-pass filter and the amplitude of the P wave measured on the record we estimate $|F(\omega)|$ by averaging over many small events with similar sizes (see uncorrected spectra shown in Figure 18). This choice of P waves was motivated by the ease with which these wavelets can be detected and measured on our records. No readings of S waves were made because of their often complex wave forms. In order to correct the resulting source spectrum for attenuation we studied the ratio of the amplitude spectral density of the P wave to the source factor of coda for the same event at a fixed frequency as a function of travel time t for various events. Since the attenuation of P wave is proportional to $(1/t)\exp(-\pi ft/Q_\alpha)$, an average Q_α over many different paths is obtained by fitting this function to the above ratio. Examples of such fits are shown in Figure 19 for Stone Canyon for two frequency bands centered at 6 and 24 Hz. Some of the scatter in the data may be accounted for by the radiation pattern at the earthquake source. (The coda source factor represents the azimuthal average of radiation.) Also of importance is the variation of Q_α related to different wave paths. However, no attempt was made in this study to correlate these variations with local geology. Reasonable fits are obtained for values of Q_α ranging between 200 and 400, with a best estimate of about 300. This value refers to an area covered by direct wave paths from earthquake foci down to 12 km as shown in Figure 12. It is consistent with the final Q structure that we use in the interpretation of the coda observations because our final structure near Stone Canyon consists of low Q around 70 in the shallowest crust and high Q around 1000 in the deeper crust. A Q_α of 300 is thus not unreasonable for the average over the depth range from 0 to 12 km. Figure 18*a* then shows the average source spectrum, corrected for attenuation, for a set of events recorded at Stone Canyon. These earthquakes occurred near the San Andreas fault roughly 15 km to the south of our station. Their magnitudes, determined by the U.S. Geological Survey, average about 1. The spectral curve, drawn through our data corrected for $Q_\alpha = 300$, shows a corner frequency f_0 at about 14 Hz and decay with frequency roughly proportional to ω^{-2} beyond the corner frequency. The spectral shape is remarkably flat at frequencies lower than 14 Hz. The value of f_0 does not noticeably change when Q_α is varied from 200 to 400. Similar corner frequencies and frequency dependence were obtained from studies of small events originating near the San Andreas, 20 km to the north of Stone Canyon. A corner frequency of 14 Hz and a high-frequency asymptote of ω^{-2} are thus taken to represent the average magnitude 1 earthquake in this region of central California.

Because P wave attenuation data were not available at

TABLE 2. Events Recorded at Oishiyama (34°05'56"N, 130°19'00"E)

Event	Date	Travel Time, s	Latitudinal Distance, km	Longitudinal Distance, km	Depth, km	Magnitude
			Series 1: 1971			
1	Aug. 26	2.2	1.84	26.72	2.67	6.3
2	Nov. 24	3.4	23.33	18.18	3.50	3.6
3	Oct. 16	3.9	23.99	15.10	3.41	2.6
4	Oct. 19	3.9	13.73	11.18	5.53	3.8
5	Dec. 3	2.0	4.34	23.82	2.58	4.1
6	April 2	2.2	14.28	19.73	2.16	3.0
7	June 1	2.2	14.34	19.70	3.01	2.0
8	April 1	2.1	14.35	19.76	0.50	3.0
9	June 19	2.5	18.33	19.91	2.42	2.6
10		3.6	26.61	21.48	5.81	3.3
11	June 19	4.1	20.75	11.82	4.18	3.0
12	Nov. 26	4.1	27.07	17.06	5.35	3.6
			Series 2: 1970			
1	July 12	3.2	−2.14	25.68	7.00	3.1
2	July 16	2.8	−2.22	28.24	1.38	2.1
3	Aug. 17	7.6	−14.44	5.63	12.41	2.1
4	Aug. 14	4.2	4.05	10.86	4.60	2.2
5	Aug. 15	3.6	12.74	12.71	5.66	3.1
6	Aug. 12	3.6	5.81	13.34	4.03	2.0
7	Aug. 12	3.2	23.94	21.00	4.97	2.1
8	Aug. 10	2.3	9.51	19.37	3.19	2.0
9	Aug. 11	5.0	−2.1	10.94	8.19	2.9
10	July 31	4.1	20.65	12.39	5.01	2.3
11	July 20	2.0	3.92	23.82	1.85	2.3
12	July 30	3.8	13.55	11.52	4.91	2.5
13	July 31	4.0	21.60	13.54	5.13	2.2
14	Aug. 2	9.1	−33.45	33.47	1.27	2.5
15	Aug. 1	2.9	15.47	16.12	0.53	1.9
16	Aug. 4	3.9	21.64	14.29	5.77	1.8
17	July 20	2.4	8.86	18.56	1.83	2.3
18	Aug. 14	24.8	71.02	138.70	7.86	3.2
19	July 29	3.4	18.88	15.32	4.31	2.0
20	July 29	2.8	7.55	17.74	5.32	2.7
21	July 27	3.7	9.66	12.30	5.75	2.9
22	July 27	6.1	−18.31	26.02	4.15	3.2
23	July 25	3.7	16.82	12.74	4.95	2.1
24	July 25	3.2	13.47	15.58	6.79	2.4
25	Aug. 5	3.3	24.86	21.20	4.91	2.1
26	Aug. 6	22.4	86.71	112.94	0.00	3.7
27	July 10	13.0	−45.51	58.07	11.91	2.7
28	Aug. 8	3.5	13.39	12.77	3.36	2.2
29	Aug. 6	4.0	5.98	12.10	6.94	2.1
30	Aug. 9	4.1	21.11	12.55	4.67	1.9
31	July 21	6.3	−18.66	26.05	6.60	2.8
32	July 31	2.8	24.31	26.45	5.47	3.1
33	Aug. 3	4.6	7.38	8.85	7.50	3.1
34	July 22	4.5	19.01	9.51	4.91	2.4
35	July 19	3.0	21.19	20.48	6.76	2.1
36	July 14	3.9	21.68	13.63	4.23	3.6
37	July 10	4.4	6.52	9.46	5.74	2.5
38	Aug. 4	3.1	−1.60	24.93	5.72	3.3
39	July 17	2.9	23.50	21.73	3.19	3.6
			Series 3: 1970			
1	July 9	9.4	−23.14	16.98	28.89	3.9
2	Aug. 8	11.5	−25.68	5.14	35.61	3.4
3	Aug. 10	11.5	−20.40	30.95	47.82	3.1
4	Aug. 6	12.2	−22.29	−3.49	37.70	2.6
5	Aug. 16	22.1	−74.17	−34.12	27.11	2.6
6	July 19	13.2	−44.60	55.21	23.58	3.8
7	Aug. 6	12.2	−18.67	−6.67	38.09	2.2
8	July 31	13.1	−29.92	−2.27	38.67	3.7
9	July 31	13.0	−26.05	4.11	46.04	3.8
10	July 23	18.4	−72.97	44.44	32.36	2.8
11	Aug. 6	18.0	−52.35	−30.33	19.71	4.6
12	July 3	10.8	−24.97	1.48	27.01	4.2

Event positions are referred to 34°N latitude and 135°E longitude. Distances north and east are positive.

TABLE 3. Events recorded at Tsukuba (36°12'39"N, 140°06'35"E)

Event	Date	Origin Time	North Latitude	East Longitude	Depth, km	Magnitude
1	June 21, 1971	07h 57m 10.9s	36°11'	139°48'	60	4.9
2	Aug. 10, 1971	10h 34m 34.7s	36°15'	139°47'	60	3.8
3	Aug. 4, 1971	00h 32m 43.7s	36°21'	140°07'	70	4.9
4	Aug. 5, 1971	16h 05m			50	3.0
5	June 29, 1971	16h 57m				2.7
6	July 2, 1971	02h 04m			59	3.5
7	July 3, 1971	01h 51m			48	2.6
8	July 11, 1971	21h 37m 17.0s			48	4.1
9	Dec. 24, 1969	04h 45m 05.3s	36°23'	140°01'	70	
10	Dec. 25, 1969	03h 10m 31.8s	36°36'	140°31'	60	3.6
11	July 27, 1971	08h 08m 39.5s	35°56'	140°08'	80	5.5
12	Aug. 12, 1971	04h 02m 06.0s	35°45'	140°05'	76	4.9
13	Aug. 12, 1971	12h 02m			75	2.8
14	Aug. 13, 1971	16h 01m			57	3.2
15	Aug. 15, 1971	15h 46m			49	3.2
16	Feb. 4, 1970	02h 14m 13.8s	36°28'	140°38'	50	3.8
17	Jan. 29, 1970	15h 03m 20.3s	35°53'	140°35'	60	5.1
18	Feb. 4, 1970	19h 17m 45.8s	36°26'	140°47'	40	4.8
19	Feb. 17, 1970	15h 24m 08.0s	36°12'	139°18'	80	
20	March 3, 1970	21h 17m 32.9s	36°15'	140°03'	50	3.2
21	March 7, 1970	07h 31m 51.7s	36°11'	140°00'	90	
22	March 9, 1970	19h 04m 55.9s	36°35'	140°33'	50	3.8
23	March 15, 1970	17h 18m 32.6s	36°02'	140°18'	40	4.6
24	March 18, 1970	01h 47m 41.6s	35°44'	140°17'	80	
25	April 28, 1970	22h 07m 57.0s	35°54'	139°37'	20	3.5
26	May 4, 1970	06h 15m 17.6s	36°23'	140°06'	70	
27	June 10, 1970	22h 54m 22.3s	36°06'	139°49'	50	4.2
28	June 16, 1970	02h 40m 41.7s	36°10'	139°56'	50	
29	July 10, 1970	06h 04m 29.1s	36°05'	140°07'	80	
30	July 11, 1970	23h 28m 15.1s	36°30'	140°35'	50	5.1
31	July 14, 1970	03h 11m 27.0s	36°12'	139°51'	60	4.0
32	July 20, 1970	21h 05m 40.0s	36°10'	140°18'	60	
33	July 21, 1970	08h 55m 51.6s	36°01'	140°01'	70	
34	July 26, 1970	03h 00m 20.0s	35°59'	140°13'	40	3.4
35	Aug. 2, 1970	15h 44m 24.4s	36°11'	139°21'	80	
36	Aug. 4, 1970	10h 30m 11.9s	35°59'	140°33'	50	3.3
37	Aug. 27, 1970	20h 53m 16.2s	36°08'	139°56'	60	3.9
38	Sept. 9, 1970	03h 22m 56.2s	36°13'	139°41'	80	
39	Sept. 9, 1970	07h 11m 13.3s	36°19'	140°31'	50	
40	Sept. 12, 1970	11h 23m 47.8s	36°24'	140°24'	60	3.0
41	Sept. 18, 1970	15h 01m 59.2s	36°06'	140°08'	70	
42	Sept. 30, 1970	03h 43m 35.6s	36°02'	139°55'	40	3.3
43	Sept. 30, 1970	04h 26m 24.3s	35°29'	139°38'	40	4.8

Origin times are referred to Japanese Standard Time.

Oishiyama, correction of the average source spectrum at this location was made by assuming a Q_α identical to that found in California. The source spectrum shown in Figure 18*b* was obtained from *P* waves of earthquakes within about 15 km from the station. The corner frequency for these events is at about 8 Hz. Their magnitude was estimated at 1.5 from the values of the moment and the total duration. The spectral curve for Oishiyama is slightly richer in high frequencies than for Stone Canyon.

Source spectra of the type shown in Figure 18 have been obtained by *Brune* [1970] and others who followed his approach [*Douglas and Ryall*, 1972; *Thatcher*, 1972; *Hanks and Wyss*, 1972; *Tucker and Brune*, 1973; *Thatcher and Hanks*, 1973]. The source spectra $|\dot{M}(\omega)|$ calculated from $|F(\omega)|$ according to (30) are shown at the bottom of Figure 21 for both regions studied.

Once the absolute value of source spectrum for the smallest earthquake is fixed, those for greater earthquakes can be obtained by using the source factor of coda amplitude relative to that of the smallest earthquake. Figure 20 shows the relation between the source factors of coda amplitude of a given earthquake at different frequencies. At the bottom the source factors at 1.5 Hz and 12 Hz are plotted for earthquakes at Oishiyama. Each point represents an earthquake. The good fit of the straight line with slope 1 implies that the spectral shape does not change with earthquake magnitude in the frequency range 1.5–12 Hz. The magnitude of the earthquakes shown in Figure 20 ranges from 1 to about 3.5.

On the other hand, the spectral shape changes with magnitude, in the magnitude range from 1 to 3, for Stone Canyon, because the rate of increase in the source factors at 12 and 24 Hz is much slower than at 1.5 Hz as shown in the top or middle of Figure 20.

We now construct a family of spectral curves superposing the relative source factor of coda amplitude over the absolute source spectrum for $M1$ earthquakes. The results are summarized in Figure 21. The strong scale effect on spectral shape observed for Stone Canyon, when superposed upon the absolute spectrum for $M1$ earthquakes, results in a decrease of corner frequency with increasing magnitude from 14 Hz down to 2 Hz at around $M3$ along path 1. On the other hand, the corner frequency is kept constant at about 8 Hz for Oishiyama as indicated by path 2. The difference between the source

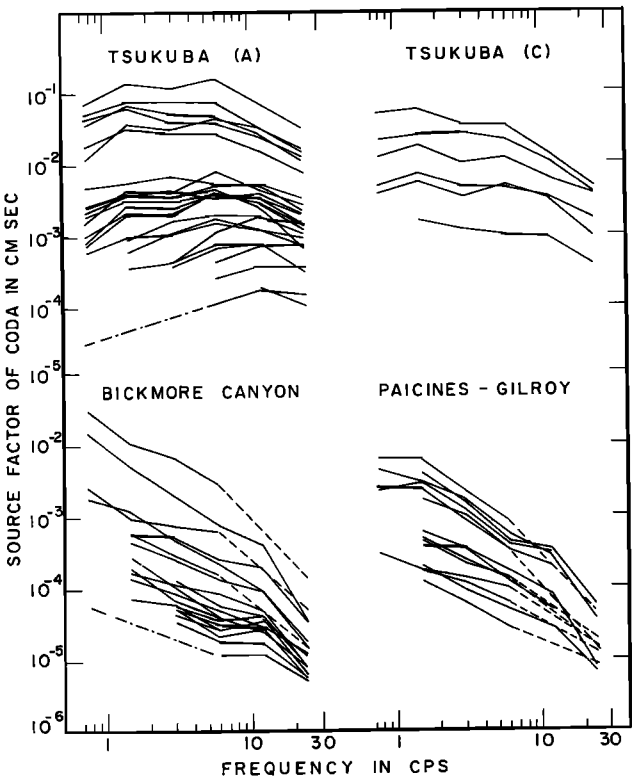

Fig. 13. Source factors of coda in the range 1–24 Hz at Tsukuba, Japan, and Stone Canyon, California. The dashed lines correspond to the cases where the midpoints are missing (no observation). There is no apparent variation in the source factors of coda waves between events in the Paicines-Gilroy region, north of Stone Canyon, and earthquakes within the Bickmore Canyon area, south of Stone Canyon. At Tsukuba the source factors of coda waves are slightly richer in high frequencies in region A than in region C (see Figure 10).

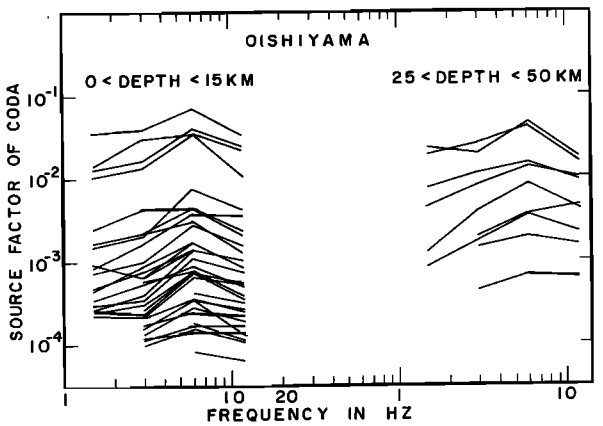

Fig. 14. Source factors of coda in the range 1–12 Hz at Oishiyama, Japan. There is no visible effect of the focal depth of earthquakes on the spectral characteristics of the source factors in this region.

spectra at Oishiyama and Stone Canyon for $M3$ earthquakes is quite striking; the 24-Hz spectral density at Oishiyama is 15 times as large as that at Stone Canyon as a result of the difference in the scaling law of spectrum.

Very strong scale effects on spectrum are found for a few earthquakes with magnitudes greater than 3 for both areas as shown in Table 6. Incorporating these effects in Figure 21 we observe that the corner frequency at Oishiyama now decreases with increasing magnitude. On the other hand, the corner frequency at Stone Canyon shows a slower rate of decrease. The corner frequency of the $M5$ event there is at about 1 Hz.

The path of corner frequency from $M1$ to $M6$ earthquakes follows a zigzag path consisting of three distinct segments for both areas: path 1 with the slope -3 expected for a constant stress drop, path 2 along the line of constant corner frequency or probably constant fault dimension, and path 3 back to the ω^2 scaling law [*Aki*, 1967, 1972] for magnitude greater than 6.

The curves for the Niigata earthquake (M_s = 7.5) and the Parkfield earthquake (M_s = 6.4, M_L = 5.5) shown in Figure 21 are schematic, except that the absolute values of the flat portion are very accurately determined [*Aki*, 1966; *Tsai and Aki*, 1969]. The reliable upper bounds given by these earthquakes and lower bounds determined for the smallest and closest earthquakes appear to divide 6.5 decades of seismic moment range into 4.5 units of local magnitudes. This is consistent with the relation of seismic moment and local magnitude obtained by *Aki* [1969], *Wyss and Brune* [1968], *Thatcher and Hanks* [1973], and *Bakun and Bufe* [1975].

We realized some inconsistency when we superposed the relative source spectra obtained from coda waves, which are probably mostly shear waves, over the P wave source spectra for $M1$ earthquakes. The discussion on the difference between P and S corner frequencies as well as on the stress drop associated with the corner frequency path in Figure 21 will be postponed to a separate paper, in preparation. In this paper we are only concerned with a rough order of magnitude estimate of the absolute value of the source spectrum of the $M3$ earthquake to be used for estimating the turbidity.

Quantitative Discussions on the Origin of Coda Waves

Let us now apply the theoretical models of coda waves discussed earlier to the observed results and see if the resultant model parameters are reasonable.

We shall first apply the single-scattering theory to the earthquakes observed at Stone Canyon. The basic equation for the theory is (17),

TABLE 4. Values of the Coefficient a in (28) Obtained From the Least Squares Computation

Event Group*	f = 0.75	f = 1.50	f = 3.00	f = 6.00	f = 12.00	f = 24.00
Stone Canyon 1	0.54 (±0.13)	1.33 (±0.10)	1.30 (±0.06)	1.02 (±0.06)	0.26 (±0.10)	−0.05 (±0.08)
Stone Canyon 2	...	0.82 (±0.21)	1.19 (±0.12)	1.48 (±0.17)	1.10 (±0.14)	1.12 (±0.16)
Stone Canyon 3	1.38 (±0.19)	2.44 (±0.16)	1.66 (±0.11)	0.98 (±0.14)	−0.36 (±0.19)	−0.64 (±0.24)
Oishiyama 1	...	2.35 (±0.15)	2.31 (±0.25)	1.21 (±0.27)	0.77 (±0.26)	...
Oishiyama 2	...	1.99 (±0.19)	1.94 (±0.13)	1.41 (±0.12)	1.12 (±0.12)	...
Oishiyama 3	...	2.91 (±0.25)	1.31 (±0.32)	3.80 (±0.37)	0.75 (±0.48)	...
Tsukuba	0.69 (±0.11)	0.99 (±0.11)	1.11 (±0.12)	1.69 (±0.20)	2.23 (±0.12)	1.74 (±0.15)

f is frequency in hertz.
* Numbers refer to series of events listed in Tables 1, 2, and 3.

TABLE 5a. Values of the Coefficient b in (28) Obtained From the Least Squares Computation With the Factor a in (28) Being Free

Event Group*	$f = 0.75$	$f = 1.50$	$f = 3.00$
Stone Canyon 1	$1.86 \times 10^{-2} (\pm 0.13 \times 10^{-2})$	$1.79 \times 10^{-2} (\pm 0.11 \times 10^{-2})$	$2.25 \times 10^{-2} (\pm 0.09 \times 10^{-2})$
Stone Canyon 2	...	$2.67 \times 10^{-2} (\pm 0.34 \times 10^{-2})$	$3.16 \times 10^{-2} (\pm 0.26 \times 10^{-2})$
Stone Canyon 3	$1.04 \times 10^{-2} (\pm 0.08 \times 10^{-2})$	$0.91 \times 10^{-2} (\pm 0.09 \times 10^{-2})$	$1.73 \times 10^{-2} (\pm 0.09 \times 10^{-2})$
Oishiyama 1	...	$0.38 \times 10^{-2} (\pm 0.13 \times 10^{-2})$	$1.08 \times 10^{-2} (\pm 0.29 \times 10^{-2})$
Oishiyama 2	...	$1.60 \times 10^{-2} (\pm 0.24 \times 10^{-2})$	$1.74 \times 10^{-2} (\pm 0.17 \times 10^{-2})$
Oishiyama 3	...	$0.33 \times 10^{-2} (\pm 0.15 \times 10^{-2})$	$1.83 \times 10^{-2} (\pm 0.20 \times 10^{-2})$
Tsukuba	$0.48 \times 10^{-2} (\pm 0.04 \times 10^{-2})$	$0.72 \times 10^{-2} (\pm 0.05 \times 10^{-2})$	$0.99 \times 10^{-2} (\pm 0.07 \times 10^{-2})$
Event Group*	$f = 6.00$	$f = 12.00$	$f = 24.00$
Stone Canyon 1	$2.85 \times 10^{-2} (\pm 0.12 \times 10^{-2})$	$4.68 \times 10^{-2} (\pm 0.23 \times 10^{-2})$	$5.27 \times 10^{-2} (\pm 0.22 \times 10^{-2})$
Stone Canyon 2	$3.14 \times 10^{-2} (\pm 0.43 \times 10^{-2})$	$3.18 \times 10^{-2} (\pm 0.36 \times 10^{-2})$	$2.85 \times 10^{-2} (\pm 0.49 \times 10^{-2})$
Stone Canyon 3	$2.99 \times 10^{-2} (\pm 0.18 \times 10^{-2})$	$5.50 \times 10^{-2} (\pm 0.30 \times 10^{-2})$	$6.60 \times 10^{-2} (\pm 0.51 \times 10^{-2})$
Oishiyama 1	$3.13 \times 10^{-2} (\pm 0.34 \times 10^{-2})$	$4.45 \times 10^{-2} (\pm 0.38 \times 10^{-2})$	...
Oishiyama 2	$3.26 \times 10^{-2} (\pm 0.19 \times 10^{-2})$	$3.97 \times 10^{-2} (\pm 0.20 \times 10^{-2})$	...
Oishiyama 3	$0.84 \times 10^{-2} (\pm 0.25 \times 10^{-2})$	$3.93 \times 10^{-2} (\pm 0.39 \times 10^{-2})$	...
Tsukuba	$1.11 \times 10^{-2} (\pm 0.12 \times 10^{-2})$	$0.86 \times 10^{-2} (\pm 0.08 \times 10^{-2})$	$1.52 \times 10^{-2} (\pm 0.12 \times 10^{-2})$

f is frequency in hertz.
* Numbers refer to series of events listed in Tables 1, 2, and 3.

$$P(\omega \mid t) = \frac{v}{2} g(\pi) |\phi_0(\omega \mid r)|^2 \qquad (17)$$

where $r = vt/2$.

For surface waves we shall use the simplest case of Rayleigh waves in a half space due to a point strike slip source [*Ben-Menahem*, 1961],

$$\phi_0(\omega | r) = 0.125 \sin 2\theta \, f(h) \dot{M}(\omega) / [\mu c_R (\lambda r)^{1/2}] \qquad (33)$$

where $\phi_0(\omega | r)$ is the Fourier transform of vertical displacement at a distance r, μ is the rigidity of the medium, c_R is the Rayleigh wave velocity, λ is the wavelength, θ is the azimuth from the fault strike, and $f(h)$ is the factor due to focal depth. Poisson's ratio is assumed to be 0.25.

Putting the above equation into (17), we find that the backward turbidity coefficient $g(\pi)$ can be determined if $t^{1/2}[P(\omega | t)]^{1/2}/M(\omega)$ is known from the observation. Since the coda amplitude recorded on our band-pass filter seismograph is related to the coda power as $A(\omega | t) = 2 [2P(\omega | t) \Delta f]^{1/2}$, the source factor determined previously by constraining $a = 0.5$ should give the necessary information. For an average earthquake with magnitude 3 at Stone Canyon, $\dot{M}(\omega)$ is 8×10^{20} dyn cm at 1 Hz. From the coda source factor of the same earthquake, on the other hand, we find that $t^{1/2}A(\omega | t)$ is 1×10^{-3} cm $s^{1/2}$ at 1 Hz. For a rough estimation of $g(\pi)$ we shall assume that $\mu = 3 \times 10^{11}$ dyn cm, $c_R = 3$ km/s, $\lambda = 3$ km, $\Delta f = 1$ Hz, and an average azimuth depth factor $\sin 2\theta \times f(h) \simeq 0.1$. Then the backward turbidity $g(\pi)$ is estimated as 3×10^{-1} per kilometer. In other words, in order to explain the observed coda as backscattering Rayleigh waves, the fractional loss of energy by scattering within the unit azimuthal angle (1 rad) in the backward direction should be $3/(20\pi)$ per 1-km travel distance.

The above value of the backward turbidity coefficient does not seem to be unreasonable when we consider the strong near-surface heterogeneity commonly shown in geology maps.

On the other hand, we have an independent check on the turbidity coefficient if we assume body wave scattering for the origin of coda waves. As discussed earlier, the model of random medium under the Montana Lasa predicts very small

TABLE 5b. Values of the Coefficient b in (28) Obtained From the Least Squares Computation With the Factor a in (28) Fixed to 1

Event Group*	$f = 0.75$	$f = 1.50$	$f = 3.00$
Stone Canyon 1	$1.43 \times 10^{-2} (\pm 0.04 \times 10^{-2})$	$2.15 \times 10^{-2} (\pm 0.05 \times 10^{-2})$	$2.67 \times 10^{-2} (\pm 0.04 \times 10^{-2})$
Stone Canyon 2	...	$2.40 \times 10^{-2} (\pm 0.14 \times 10^{-2})$	$3.51 \times 10^{-2} (\pm 0.12 \times 10^{-2})$
Stone Canyon 3	$1.19 \times 10^{-2} (\pm 0.04 \times 10^{-2})$	$1.56 \times 10^{-2} (\pm 0.06 \times 10^{-2})$	$2.17 \times 10^{-2} (\pm 0.06 \times 10^{-2})$
Oishiyama 1	...	$1.43 \times 10^{-2} (\pm 0.07 \times 10^{-2})$	$2.47 \times 10^{-2} (\pm 0.12 \times 10^{-2})$
Oishiyama 2	...	$2.77 \times 10^{-2} (\pm 0.09 \times 10^{-2})$	$2.92 \times 10^{-2} (\pm 0.07 \times 10^{-2})$
Oishiyama 3	...	$1.41 \times 10^{-2} (\pm 0.04 \times 10^{-2})$	$2.02 \times 10^{-2} (\pm 0.06 \times 10^{-2})$
Tsukuba	$0.38 \times 10^{-2} (\pm 0.02 \times 10^{-2})$	$0.72 \times 10^{-2} (\pm 0.02 \times 10^{-2})$	$1.05 \times 10^{-2} (\pm 0.02 \times 10^{-2})$
Event Group*	$f = 6.00$	$f = 12.00$	$f = 24.00$
Stone Canyon 1	$2.89 \times 10^{-2} (\pm 0.05 \times 10^{-2})$	$3.11 \times 10^{-2} (\pm 0.09 \times 10^{-2})$	$2.59 \times 10^{-2} (\pm 0.09 \times 10^{-2})$
Stone Canyon 2	$4.23 \times 10^{-2} (\pm 0.18 \times 10^{-2})$	$3.42 \times 10^{-2} (\pm 0.13 \times 10^{-2})$	$3.19 \times 10^{-2} (\pm 0.17 \times 10^{-2})$
Stone Canyon 3	$2.97 \times 10^{-2} (\pm 0.09 \times 10^{-2})$	$3.52 \times 10^{-2} (\pm 0.13 \times 10^{-2})$	$3.26 \times 10^{-2} (\pm 0.17 \times 10^{-2})$
Oishiyama 1	$3.39 \times 10^{-2} (\pm 0.11 \times 10^{-2})$	$4.14 \times 10^{-2} (\pm 0.13 \times 10^{-2})$	...
Oishiyama 2	$3.84 \times 10^{-2} (\pm 0.07 \times 10^{-2})$	$4.16 \times 10^{-2} (\pm 0.06 \times 10^{-2})$	...
Oishiyama 3	$2.63 \times 10^{-2} (\pm 0.08 \times 10^{-2})$	$3.73 \times 10^{-2} (\pm 0.09 \times 10^{-2})$	...
Tsukuba	$1.50 \times 10^{-2} (\pm 0.05 \times 10^{-2})$	$1.57 \times 10^{-2} (\pm 0.03 \times 10^{-2})$	$2.03 \times 10^{-2} (\pm 0.04 \times 10^{-2})$

f is frequency in hertz.
* Numbers refer to series of events listed in Tables 1, 2, and 3.

TABLE 5c. Values of the Coefficient b in (28) Obtained From the Least Squares Computation With the Factor a in (28) Fixed to 0.5

Event Group*	$f = 0.75$	$f = 1.50$	$f = 3.00$
Stone Canyon 1	$1.89 \times 10^{-2} (\pm 0.03 \times 10^{-2})$	$2.70 \times 10^{-2} (\pm 0.05 \times 10^{-2})$	$3.37 \times 10^{-2} (\pm 0.05 \times 10^{-2})$
Stone Canyon 2	...	$3.15 \times 10^{-2} (\pm 0.14 \times 10^{-2})$	$4.44 \times 10^{-2} (\pm 0.13 \times 10^{-2})$
Stone Canyon 3	$1.38 \times 10^{-2} (\pm 0.05 \times 10^{-2})$	$1.79 \times 10^{-2} (\pm 0.07 \times 10^{-2})$	$2.51 \times 10^{-2} (\pm 0.07 \times 10^{-2})$
Oishiyama 1	...	$1.82 \times 10^{-2} (\pm 0.07 \times 10^{-2})$	$3.01 \times 10^{-2} (\pm 0.12 \times 10^{-2})$
Oishiyama 2	...	$3.36 \times 10^{-2} (\pm 0.10 \times 10^{-2})$	$3.55 \times 10^{-2} (\pm 0.07 \times 10^{-2})$
Oishiyama 3	...	$1.69 \times 10^{-2} (\pm 0.05 \times 10^{-2})$	$2.32 \times 10^{-2} (\pm 0.06 \times 10^{-2})$
Tsukuba	$0.54 \times 10^{-2} (\pm 0.02 \times 10^{-2})$	$0.92 \times 10^{-2} (\pm 0.02 \times 10^{-2})$	$1.31 \times 10^{-2} (\pm 0.03 \times 10^{-2})$
Event Group*	**$f = 6.00$**	**$f = 12.00$**	**$f = 24.00$**
Stone Canyon 1	$3.73 \times 10^{-2} (\pm 0.05 \times 10^{-2})$	$4.17 \times 10^{-2} (\pm 0.08 \times 10^{-2})$	$3.86 \times 10^{-2} (\pm 0.08 \times 10^{-2})$
Stone Canyon 2	$5.35 \times 10^{-2} (\pm 0.20 \times 10^{-2})$	$4.59 \times 10^{-2} (\pm 0.14 \times 10^{-2})$	$4.59 \times 10^{-2} (\pm 0.18 \times 10^{-2})$
Stone Canyon 3	$3.52 \times 10^{-2} (\pm 0.09 \times 10^{-2})$	$4.25 \times 10^{-2} (\pm 0.12 \times 10^{-2})$	$4.28 \times 10^{-2} (\pm 0.16 \times 10^{-2})$
Oishiyama 1	$4.00 \times 10^{-2} (\pm 0.11 \times 10^{-2})$	$4.82 \times 10^{-2} (\pm 0.13 \times 10^{-2})$	...
Oishiyama 2	$4.55 \times 10^{-2} (\pm 0.07 \times 10^{-2})$	$4.93 \times 10^{-2} (\pm 0.07 \times 10^{-2})$	...
Oishiyama 3	$2.95 \times 10^{-2} (\pm 0.08 \times 10^{-2})$	$4.13 \times 10^{-2} (\pm 0.09 \times 10^{-2})$	...
Tsukuba	$1.79 \times 10^{-2} (\pm 0.05 \times 10^{-2})$	$1.86 \times 10^{-2} (\pm 0.04 \times 10^{-2})$	$2.38 \times 10^{-2} (\pm 0.04 \times 10^{-2})$

f is frequency in hertz.
* Numbers refer to series of events listed in Tables 1, 2, and 3.

backward turbidity coefficients (8×10^{-5} km^{-1} for $N(r) = e^{-r/a}$ and 2.5×10^{-12} km^{-1} or less for $N(r) = e^{-r^2/a^2}$) for P waves with frequencies higher than 0.5 Hz.

For body waves we shall consider the simplest case of an unbounded homogeneous medium [e.g., *Maruyama*, 1963],

$$\phi_0(\omega \mid r) = \frac{\dot{M}(\omega)}{4\pi v^3 \rho} \frac{1}{(2)^{1/2}} \cdot \frac{1}{r} \tag{34}$$

where v is the propagation velocity and $1/(2)^{1/2}$ stands for an average of the geometrical factor. Putting the above equation into (17), we find that the backward turbidity coefficient $g(\pi)$ can be determined if $t[P(\omega \mid t)]^{1/2}/M(\omega)$ is known from observation. The source factor of coda amplitude determined by constraining $a = 1.0$ should give the necessary information. For an average earthquake with magnitude 3 at Stone Canyon, $tA(\omega \mid t)$ is 4×10^{-3} cm s at 1 Hz. The corresponding value of $\dot{M}(\omega)$ is 8×10^{20} dyn cm as given before.

For a rough estimate of backward turbidity coefficient $g(\pi)$, putting $\rho = 3$ g cm^{-3}, $\Delta f = 1$ Hz, and $v = (10)^{1/2}$ km/s for

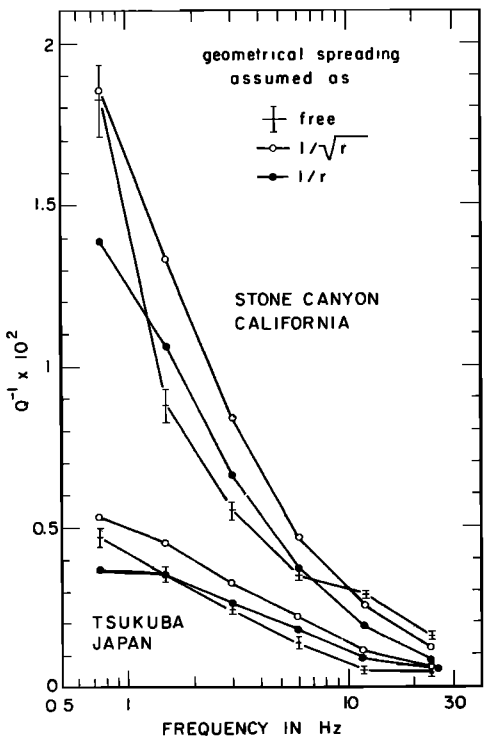

Fig. 15. Regional variations of Q^{-1} in the range 1–24 Hz derived from the analysis of earthquake coda at Tsukuba (bottom) and Stone Canyon (top), with different assumptions on the spreading mode of waves in the single-scatterer model. Open circles refer to the assumption of surface wave scattering, and closed circles refer to the assumption of body wave scattering. Crosses with error bars refer to no constraint on the mode. The values of Q^{-1} derived from the diffusion model would fall in between the values shown for surface wave and body wave assumptions.

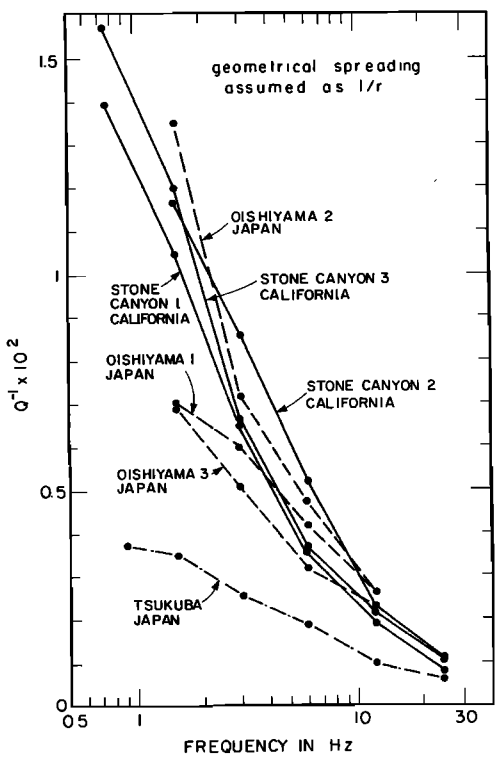

Fig. 16. Regional variations of Q^{-1} in the range 1–24 Hz derived from the analysis of earthquake coda at Tsukuba, Oishiyama, and Stone Canyon. The values shown were derived from the single-scattered model assuming body wave scattering. Numbers, attached to each region, refer to the series of events listed in Tables 1, 2, and 3.

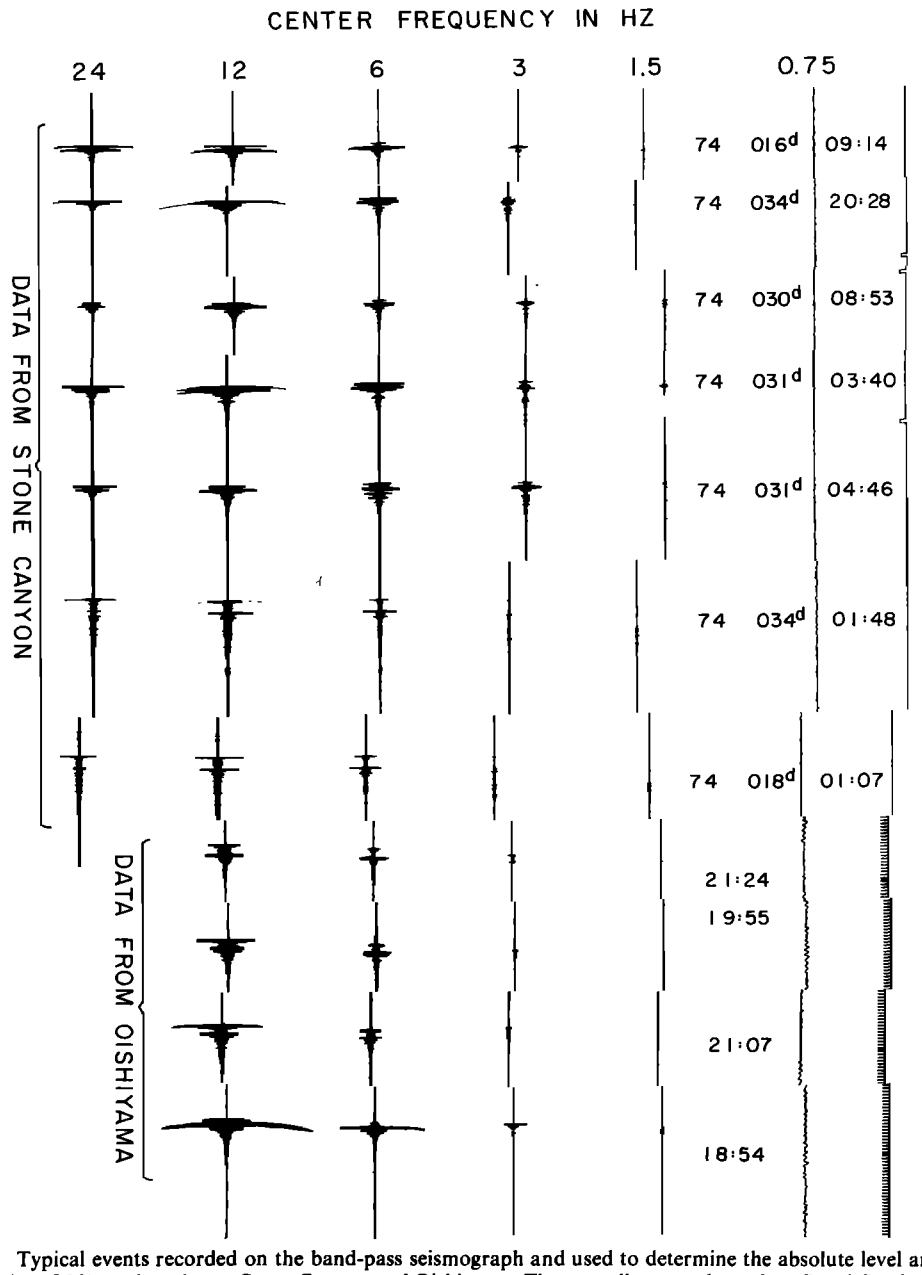

Fig. 17. Typical events recorded on the band-pass seismograph and used to determine the absolute level and spectral characteristics of $M1$ earthquakes at Stone Canyon and Oishiyama. These small events show clear P and S pulses with very little scattering, thereby suggesting the applicability of the direct deterministic analysis.

shear waves, we find $g(\pi)$ to be about 0.14 km^{-1}. For compressional waves, $g(\pi)$ is as much as 6 km^{-1}. These backward turbidity coefficients are many orders of magnitude larger than the values estimated earlier from the parameters of the random medium model under Lasa. In other words, the heterogeneity of the lithosphere determined from the fluctuation of amplitude and phase spectra of teleseismic P waves at Lasa is not strong enough to account for the coda of local earthquakes as backscattering body waves.

In order to substantiate the above conclusion we shall apply the three-dimensional diffusion model corresponding to body wave scattering of the same earthquake. First, by eliminating the attenuation effect from the basic equation (13),

$$P(\omega \mid t) = \frac{W(\omega)}{\rho\omega^2(4\pi Dt)^{3/2}} \tag{35}$$

In order to determine the diffusivity D we first find the source factor of coda amplitude constraining $a = 0.75$. This gives $t^{3/4}A(\omega|t)$ and therefore $t^{3/2}P(\omega|t)$; $W(\omega)$ is the total seismic energy within a unit frequency band around ω. The total seismic energy is estimated by the Gutenberg-Richter formula $\log E = 11.8 + 1.5\,M$. Then the fractional energy within a given frequency band is estimated from the source spectrum as shown in Figure 21, where we extended the low-frequency side by a flat straight line and the high-frequency side by the ω^{-2} line. For $M3$ earthquakes at Stone Canyon the energy in the 1-Hz band was estimated as 2.1×10^{15} ergs. The value of $t^{3/4}A(\omega|t)$ for the same band was 1.7×10^{-3} cm s$^{3/4}$. Putting these values into (35), we obtain $D = 10^{12}$ cm^2 s^{-1}. Then, using (20) and assuming shear velocity of 3 km/s, we find that the mean free path is 10^7 cm or 100 km, or the turbidity coefficient is 10^{-2} km^{-1}.

For the body waves around 1 Hz in the random media assumed under Lasa, most of the scattered energy is directed

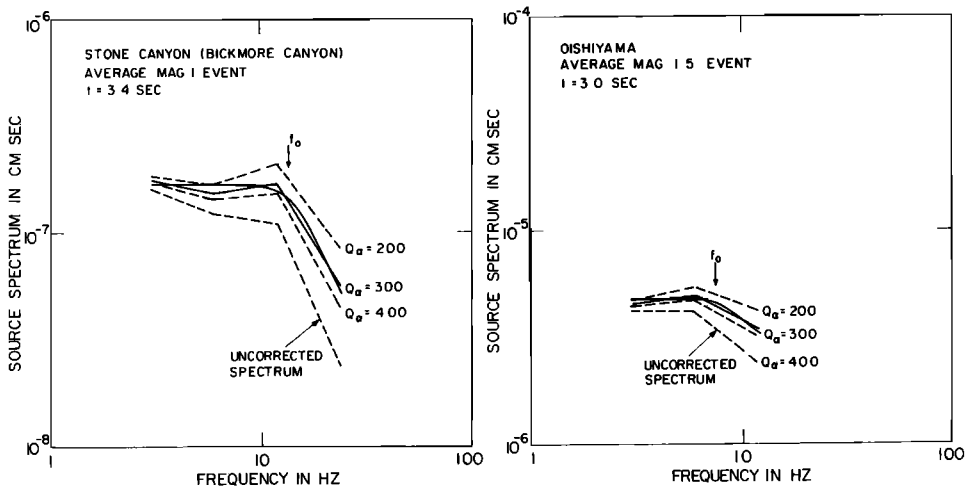

Fig. 18. Average source spectra, corrected for attenuation, of the smallest and closest events recorded at Stone Canyon and Oishiyama.

forward because of large *ka* [*Aki*, 1973]. The parts of scattered energy for which the diffusion theory may be applicable are probably only those scattered in a backward direction. Therefore the turbidity coefficient obtained from diffusivity should be considered as a rough estimate of backward turbidity. The value obtained from coda is again several orders of magnitude greater than that estimated for the random medium under Lasa. Thus we conclude that the heterogeneity of lithosphere is not strong enough to explain observed coda waves at around 1 Hz as backscattering body waves. They must be primarily backscattering surface waves, with the backward turbidity $g(\pi)$ of the order of 3×10^{-1} km^{-1}.

The same analysis was extended to higher frequencies as well as to other stations. The results for body wave scattering are summarized in Tables 7 and 8. The low turbidity for Tsukuba may be due to the deeper focal depth and consequently less surface wave scattering, although we had to assume the same source spectrum as Oishiyama due to the lack of observed absolute spectrum there.

In a previous section we suggested that the apparent frequency dependence of Q of coda waves may be due to the strong variation of Q with depth. The low-frequency coda waves around 1 Hz may be backscattering surface waves propagating mostly in the low-Q shallow part of the earth's crust, and the high-frequency coda around 20 Hz may be backscattering body waves from heterogeneities in the deep lithosphere.

The results of this section support the above suggestion, because we showed that the low-frequency coda waves cannot be backscattering body waves especially at Stone Canyon and Oishiyama. At Tsukuba, where earthquakes are deeper and less surface wave scattering is expected, the turbidity is low and Q is high, consistent with our supposition.

The observed high Q for high-frequency coda, on the other

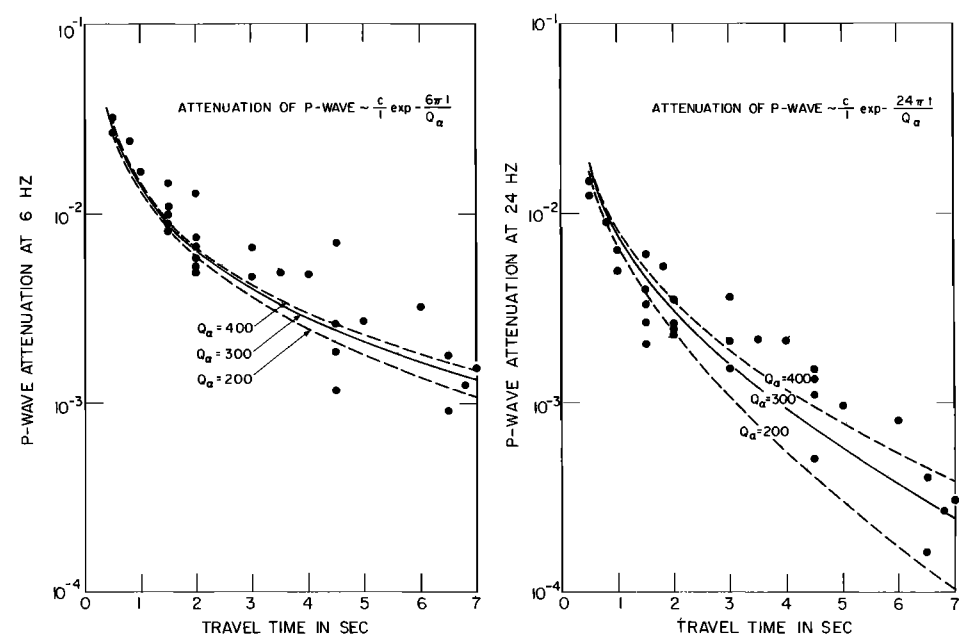

Fig. 19. Attenuation of P wave at 6 and 24 Hz in central California. Each data point represents the ratio of the amplitude spectral density of the P wave to the source factor of coda waves at the given frequency for a given earthquake. Solid and dashed lines are fits obtained with the function $(c/t) \exp(-\pi f t/Q_\alpha)$ for different values of Q_α.

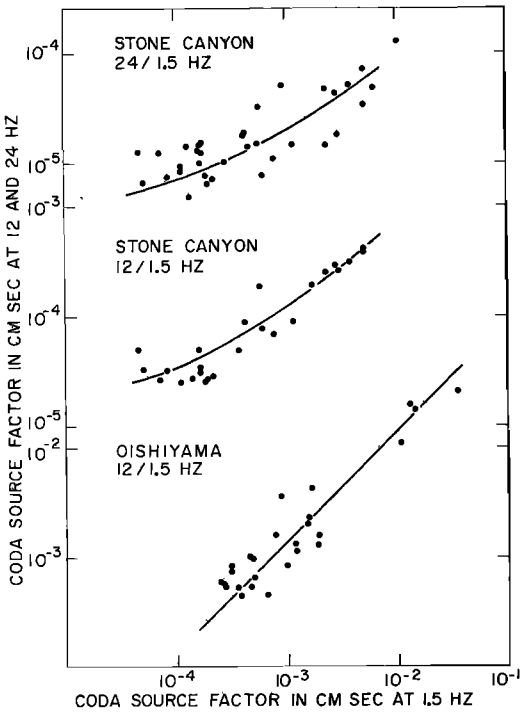

Fig. 20. Relation between the growth of source spectral densities at different frequencies. At Stone Canyon the rate of increase of spectrum at 12 and 24 Hz is much slower than that at 1.5 Hz. On the other hand, the same rate is observed for 12 and 1.5 Hz at Oishiyama, indicating no change in spectral shape with increasing magnitude at least in the frequency range from 1.5 to 12 Hz. The smooth curves drawn through the data points are obtained from the relative amplitudes of corresponding spectral curves shown in Figure 21.

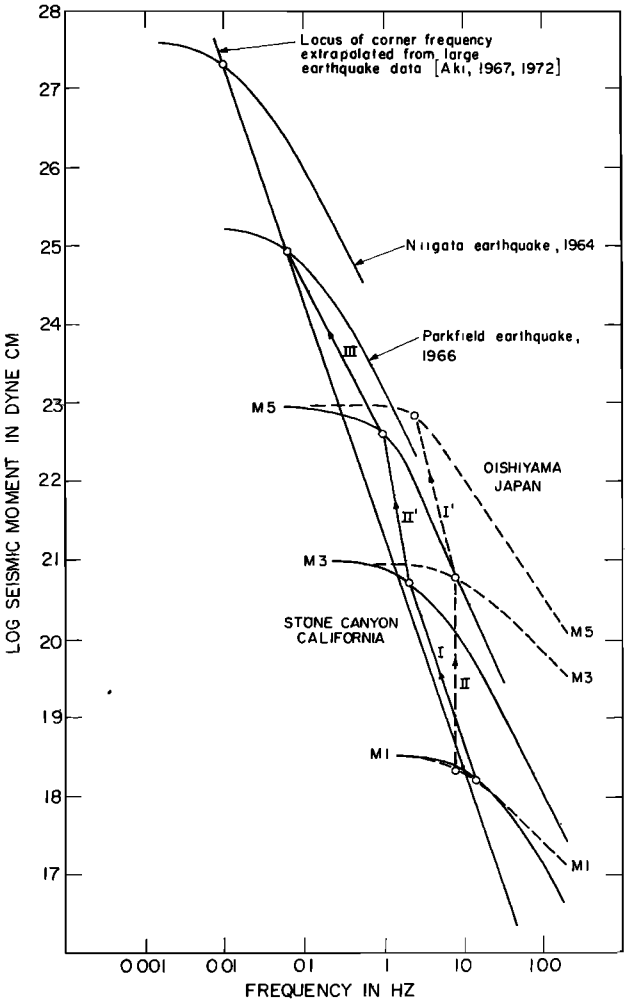

Fig. 21. Starting with magnitude 1 ($M1$) earthquake, the growth of seismic source spectrum with magnitude is shown for two seismic areas: one in western Japan, the other in central California. The seismic moment corresponding to each spectral curve is indicated at the low-frequency end. The locus of the corner frequency appears to consist of three segments: (1) segment with slope of -3 expected for the similarity assumption underlying the ω^2 law, (2) segment along the line of constant corner frequency reflecting an inhomogeneity length characteristic to the earth's crust in the area, (3) segment going back to the ω^2 law applicable to earthquakes larger than $M6$. The curves for the Niigata earthquake (M_s = 7.5) and the Parkfield earthquake (M_s = 6.4) are schematic, except that absolute values of the flat portion are very accurately determined to give reliable upper bounds for seismic moment estimate.

hand, eliminates the possibility that they are backscattering surface waves confined in the low-Q shallow depth. They must be backscattering body waves from heterogeneities in the deep lithosphere.

The value of backward turbidity required to explain them as backscattering body waves is $10^{-2} \sim 10^{-3}$ km^{-1} for all the stations. If we use (18), one can determine the ratio $\langle\mu^2\rangle/a$. The required backward turbidity may then be explained by assuming the correlation distance a = 0.1 ~ 1 km and $\langle\mu^2\rangle^{1/2}$ = 4%. Although this result is not uniquely determined, such a small-scale inhomogeneity, if it exists under Lasa, may give negligible effects on teleseismic body waves with frequency around 1 Hz or be masked by the effects of larger-scale inhomogeneity. Thus there are no observations against the idea that the high-frequency coda waves are backscattering body waves from heterogeneities in the deep lithosphere.

Conclusions

We proposed a method of determining the source spectra of small local earthquakes from their coda waves. The basic assumption underlying our technique is that the coda spectra are independent of epicentral distance and details of the direct wave path from source to station. The existence of a common shape of coda amplitude decay curve (Figures 7, 8, and 9) supports that assumption.

Two extreme models of the wave medium were proposed to account for the observation made on the coda waves. Both models are based on the idea that the coda waves are backscattering waves from numerous heterogeneities distributed uniformly in the earth's crust. In the first model the scattering was assumed to be a weak process, and use was made of the Born approximation. Because of this approximation the law of conservation of energy was violated. To alleviate this problem, a

TABLE 6. Spectral Ratios

Frequency, Hz	Magnitude Ratios		
	4.4/3.5*	5.5/4.4*	5/4†
0.75	10	55	13
1.5	8	50	10
3	5	22	9
6	3	20	3
12	2	16	2
24	...	15	1.5

* Values for Oishiyama.
† Value for Stone Canyon.

TABLE 7. Coda Source Factor and Seismic Moment for Earthquakes with Magnitude 3

Station	Frequency f, Hz	Coda Source Factor $A(\omega\|t)t$, cm s	Moment* $\dot{M}(\omega)$, dyn cm	Turbidity $g(\pi)$, km^{-1}
Stone Canyon	1	4.0×10^{-3}	8.0×10^{20}	0.140
	24	3.5×10^{-5}	1.7×10^{19}	0.002
Oishiyama	1	5.5×10^{-4}	8.0×10^{20}	0.003
	12	5.5×10^{-4}	4.4×10^{20}	0.001
Tsukuba	1	3.0×10^{-4}	8×10^{20}†	0.001
	24	3.0×10^{-4}	10^{20}†	0.003

Interpretation by the single-scattering theory for body waves.
* More precisely, this is the spectral density of the time derivative of seismic moment.
† Source spectrum assumed to be the same as for Oishiyama.

TABLE 8. Coda Source Factor and Seismic Energy for Earthquakes With Magnitude 3

Station	Frequency, Hz	Coda Source Factor $t^{3/4}A(\omega\|t)$, $cm\ s^{3/4}$	Square Root of Energy Within the Band, $ergs^{1/2}$	Diffusivity, $cm^2\ s^{-1}$	Turbidity, km^{-1}
Stone Canyon	1	1.7×10^{-3}	0.46×10^{8}	10^{12}	10^{-2}
	24	2.9×10^{-5}	0.34×10^{8}	1.5×10^{13}	6.5×10^{-4}
Oishiyama	1	0.6×10^{-3}	0.20×10^{8}	1.3×10^{12}	7.4×10^{-3}
	12	0.6×10^{-3}	0.64×10^{8}	9.7×10^{11}	10^{-2}
Tsukuba	1	0.5×10^{-4}	0.20×10^{8}*	3.7×10^{13}	2.7×10^{-4}
	24	0.7×10^{-4}	0.48×10^{8}*	7.3×10^{12}	1.4×10^{-3}

Interpretation by the diffusion theory.
* Source spectrum assumed to be the same as for Oishiyama.

second model was considered in which the seismic energy transfer was considered as a diffusion process. In this strong scattering model the energy was of course conserved, but the exact partitioning of seismic energy between the forward and backward scattering modes remained undefined. The inadequacy of these two models in dealing with the energy balance is a reflection of their extreme simplicity. Despite these difficulties, however, we feel that they offer a basis from which a quantitative description of the origin of coda waves can be made. If the value of turbidity previously derived by *Aki* [1973] for the lithosphere under the Montana Lasa also applies to the lithosphere under Japan and California, the coda waves at around 1 Hz cannot be explained as backscattering body waves from heterogeneities in the lithosphere. We concluded that the coda waves at this frequency are primarily backscattering surface waves. The low Q found for these waves supports this assumption. On the other hand, the high Q found for waves at frequencies higher than 10 Hz strongly suggests that at these frequencies the coda is made of backscattering body waves from the deep high-Q lithosphere.

The turbidities required to explain the coda waves at frequencies higher than 10 Hz as backscattering body waves are of the order of 10^{-2}–10^{-3} km^{-1}, which may correspond to scatterer sizes in the range 0.1–1 km for a fractional rms velocity fluctuation of a few percent.

Acknowledgments. We are grateful to Masaru Tsujiura of Tokyo University for making the data from Tsukuba and Oishiyama available to us; to Jerry Eaton, Jack Healy, and Dick Thompson of the U.S. Geological Survey for their help with the operation at Stone Canyon; to Eystein Husebye for the coda record obtained at Norsar; and to Sara Brydges and Dorothy Frank for their help with the preparation of the manuscript. This work was supported partially by the U.S. Geological Survey under contract 14-08-0001-13459, by the National Science Foundation under contract GA 36128X1, and by the Advanced Research Project Agency, monitored by the Air Force Office of Scientific Research, under contract F 44620-71-C-0049.

REFERENCES

Aki, K., Correlogram analyses of seismograms by means of a simple automatic computer, *J. Phys. Earth, 4,* 71–79, 1956.
Aki, K., Generation and propagation of G waves from the Niigata earthquake of June 16, 1964, *Bull. Earthquake Res. Inst. Tokyo Univ., 44,* 23–88, 1966.
Aki, K., Scaling law of seismic spectrum, *J. Geophys. Res., 72,* 1217–1231, 1967.
Aki, K., Analysis of the seismic coda of local earthquakes as scattered waves, *J. Geophys. Res., 74,* 615–631, 1969.
Aki, K., Scaling law of earthquake source time-function, *Geophys. J. Roy. Astron. Soc., 31,* 3–25, 1972.
Aki, K., Scattering of P waves under the Montana Lasa, *J. Geophys. Res., 78,* 1334–1346, 1973.
Aki, K., and M. Tsujiura, Correlation study of near earthquake waves, *Bull. Earthquake Res. Inst. Tokyo Univ., 37,* 207–232, 1959.
Aki, K., M. Tsujiura, M. Hori, and K. Goto, Spectral study of near earthquake waves, *Bull. Earthquake Res. Inst. Tokyo Univ., 36,* 71–98, 1958.
Bakun, W. H., and C. G. Bufe, Shear-wave attenuation along the San Andreas fault zone in central California, *Bull. Seismol. Soc. Amer., 65,* 439–459, 1975.
Ben-Menahem, A., Radiation of seismic surface-waves from finite moving sources, *Bull. Seismol. Soc. Amer., 51,* 401–435, 1961.
Bisztricsany, E. A., A new method for the determination of the magnitude of earthquakes, *Geofiz. Kozlem., 7,* 2, 1958.
Brune, J. N., Tectonic stress and the spectra of seismic shear waves from earthquakes, *J. Geophys. Res., 75,* 4997–5009, 1970.
Capon, J., High-resolution frequency-wave number spectrum analysis, *Proc. IEEE, 57,* 1408–1418, 1969.
Capon, J., Characterization of crust and upper mantle structure under Lasa as a random medium, *Bull. Seismol. Soc. Amer., 64,* 235–266, 1974.
Chernov, L. A., *Wave Propagation in a Random Medium,* pp. 35–57, McGraw-Hill, New York, 1960.
Cleary, J. R., and R. A. W. Haddon, Seismic wave scattering near the core-mantle boundary: A new interpretation of precursors to *PKIKP, Nature, 240,* 549–550, 1972.

Clowes, R. M., and E. R. Kanasewich, Seismic attenuation and the nature of reflecting horizons within the crust, *J. Geophys. Res., 75*, 6693–6705, 1970.

Dainty, A., M. N. Toksöz, K. R. Anderson, P. J. Pines, Y. Y. Nakamura, and G. Latham, Seismic scattering and shallow structure of the moon in Oceanus Procellarum, *Moon, 9*, 11–29, 1974*a*.

Dainty, A. M., P. J. Pines, and M. N. Toksöz, Strong scattering of seismic waves: Examples from model experiments and the moon (abstract), *Eos Trans. AGU, 55*, 362, 1974*b*.

Douglas, B. M., and A. Ryall, Spectral characteristics and stress drop for microearthquakes near Fairview Peak, Nevada, *J. Geophys. Res., 77*, 351–359, 1972.

Dunkin, J. W., Scattering of transient, spherical *P* waves by a randomly inhomogeneous elastic half-space, *Geophysics, 34*, 357–382, 1969.

Greenfield, R. J., Short-period *P* wave generation by Rayleigh wave scattering at Novaya Zemlya, *J. Geophys. Res., 76*, 7988–8002, 1971.

Haddon, R. A. W., Corrugations on the mantle-core boundary or transition layers between inner and outer cores? (abstract), *Eos Trans. AGU, 53*, 600, 1972.

Hanks, T. C., and M. Wyss, The use of body-wave spectra in the determination of seismic source parameters, *Bull. Seismol. Soc. Amer., 62*, 561–590, 1972.

Howe, M. S., Wave propagation in random media, *J. Fluid Mech., 45*(4), 769–783, 1971.

Howe, M. S., Conservation of energy in random media, with application to the theory of sound absorption by an inhomogeneous flexible plate, *Proc. Roy. Soc., Ser. A, 331*, 479–496, 1973*a*.

Howe, M. S., On the kinetic theory of wave propagation in random media, *Phil. Trans. Roy. Soc. London, Ser. A., 274*, 523–549, 1973*b*.

King, D. W., R. A. W. Haddon, and J. R. Cleary, Evidence for seismic wave scattering in the *D''* layer, *Earth Planet. Sci. Lett., 20*, 353–356, 1973.

Lee, W. H. K., R. E. Bennett, and K. L. Meagher, A method of estimating magnitude of local earthquakes from signal duration, open file report, 28 pp., Nat. Center for Earthquake Res., U.S. Geol. Surv., Menlo Park, Calif., 1972.

Levin, F. K., and D. J. Robinson, Scattering by a random field of surface scatterers, *Geophysics, 34*, 170–179, 1969.

Maruyama, T., On the force equivalents of dynamic elastic dislocations with reference to the earthquake mechanism, *Bull. Earthquake Res. Inst. Tokyo Univ., 41*, 467–486, 1963.

Nakamura, Y., G. V. Latham, M. Ewing, and J. Dorman, Lunar seismic energy transmissions (abstract), *Eos Trans AGU, 51*, 776, 1970.

Nikolayev, A. V., Seismic properties of weakly heterogeneous media, *Izv. Acad. Sci. USSR Phys. Solid Earth, 2*, 83–87, 1968.

Nikolayev, A. V., and F. S. Tregub, A statistical model of the earth's crust: Method and results, *Tectonophysics, 10*, 573–578, 1970.

O'Neill, M. E., and J. H. Healy, Determination of source parameters of small earthquakes from *P*-wave rise time, *Bull. Seismol. Soc. Amer., 63*, 599–614, 1973.

Scheimer, J., and T. E. Landers, Short-period coda of a local event at Lasa, Seismic Discrimination, *Semiannu. Tech. Sum. 42*, Lincoln Lab., Mass. Inst. of Technol., Cambridge, 1974.

Soloviev, S. L., Seismicity of Sakhalin, *Bull. Earthquake Res. Inst. Tokyo Univ., 43*, 95–102, 1965.

Takano, K., Analysis of seismic coda waves of ultramicroearthquakes in the Matsushiro area—A comparison with Parkfield, California, *J. Phys. Earth, 19*, 209–216, 1971.

Thatcher, W., Regional variations of seismic source parameters in the northern Baja California area, *J. Geophys. Res., 77*, 1549–1565, 1972.

Thatcher, W., and T. C. Hanks, Source parameters of southern California earthquakes, *J. Geophys. Res., 78*, 8547–8576, 1973.

Tsai, Y. B., and K. Aki, Simultaneous determination of the seismic moment and attenuation of seismic surface waves, *Bull. Seismol. Soc. Amer., 59*, 275–287, 1969.

Tsujiura, M., Frequency analysis of seismic waves, 1, *Bull. Earthquake Res. Inst. Tokyo Univ., 44*, 873–891, 1966.

Tsujiura, M., Frequency analysis of seismic waves, 2, *Bull. Earthquake Res. Inst. Tokyo Univ., 45*, 973–995, 1967.

Tsujiura, M., Regional variation of *P*-wave spectra, 1, *Bull. Earthquake Res. Inst. Tokyo Univ., 47*, 613–633, 1969.

Tsumura, K., Determination of earthquake magnitude from total duration of oscillation, *Bull. Earthquake Res. Inst. Tokyo Univ., 45*, 7–18, 1967.

Tucker, B. E., and J. N. Brune, *S*-wave spectra and source parameters for aftershocks of the San Fernando earthquake of February 9, 1971, in *Geological and Geophysical Studies*, vol. 3, *San Fernando Earthquake of February 9, 1971*, National Oceanic and Atmospheric Administration, Washington, D. C., 1973.

Wesley, J. P., Diffusion of seismic energy in the near range, *J. Geophys. Res., 70*, 5099–5106, 1965.

Wyss, M., and J. N. Brune, Seismic moment, stress and source dimensions for earthquakes in the California-Nevada region, *J. Geophys. Res., 73*, 4681–4694, 1968.

(Received December 6, 1974;
revised April 10, 1975;
accepted April 18, 1975.)